DTIC COPY

LOCATION, CHARACTERIZATION AND QUANTIFICATION OF HYDROACOUSTIC SIGNALS IN THE INDIAN OCEAN

M. Tolstoy
D.R. Bohnenstiehl

Lamont-Doherty Earth Observatory of
Columbia University
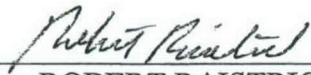61 Route 9W
Palisades, NY 10964-8000

October 2004

Final Report

AIR FORCE RESEARCH LABORATORY
Space Vehicles Directorate
29 Randolph Rd
AIR FORCE MATERIEL COMMAND
Hanscom AFB, MA 01731-3010

This technical report has been reviewed and is approved for publication.

Robert Raistrick (signature)

_____
ROBERT RAISTRICK
Contract Manager

Robert Beland (signature)

_____
ROBERT BELAND
Branch Chief

REPORT DOCUMENTATION PAGE

1. REPORT DATE (DD-MM-YYYY)	2. REPORT TYPE	3. DATES COVERED (From - To)
08-10-2004	FINAL	26 Sep 2001 – 25 Sep 2004

4. TITLE AND SUBTITLE

Location, Characterization and Quantification of Hydroacoustic Signals in the Indian Ocean

5a. CONTRACT NUMBER
DTRA01-01-C-0070

5b. GRANT NUMBER

5c. PROGRAM ELEMENT NUMBER

6. AUTHOR(S)
M. Tolstoy and D. R. Bohnenstiehl

5d. PROJECT NUMBER
DTRA

5e. TASK NUMBER
OT

5f. WORK UNIT NUMBER
A1

7. PERFORMING ORGANIZATION NAME(S) AND ADDRESS(ES)

Lamont-Doherty Earth Observatory of Columbia University
61 Route 9W
Palisades, NY 10964-8000

8. PERFORMING ORGANIZATION REPORT NUMBER

9. SPONSORING / MONITORING AGENCY NAME(S) AND ADDRESS(ES)
Air Force Research Laboratory
29 Randolph Road
Hanscom AFB, MA 01731-3010

Contract Manager: R. Raistrick AFRL/VSBYE

10. SPONSOR/MONITOR'S ACRONYM(S)
AFRL

11. SPONSOR/MONITOR'S REPORT NUMBER(S)
AFRL-VS-HA-TR-2004-1165

12. DISTRIBUTION / AVAILABILITY STATEMENT
Approved for Public Release; Distribution Unlimited.

13. SUPPLEMENTARY NOTES
The views, opinions and/or findings contained in this report are those of the author(s) and should not be construed as an official Department of the Air Force position, policy or decision, unless so designated by other documentation.

14. ABSTRACT

In this final report we summarize research accomplished on the project titled, 'Location, Characterization and Quantification of Hydroacoustic Signals in the Indian Ocean'. Our initial goals were to locate, characterize and quantify hydroacoustic signals recorded on the three available hydroacoustic stations in the Indian Ocean, and this was accomplished for available data through May 2003. However, shortly thereafter our contract was rescoped to focus on high frequency propagation through the convergence zone and blockage. Therefore our work includes results from the 2002 characterization and quantification of observed signals, as well as a detailed analysis of high frequency ice-related signals originating from Antarctica and the blockage of high frequency energy associated with a particularly large earthquake.

15. SUBJECT TERMS
Hydroacoustic signals   Seismic propagation
Seismic velocity   Seismic attenuation

16. SECURITY CLASSIFICATION OF:

a. REPORT	b. ABSTRACT	c. THIS PAGE	17. LIMITATION OF ABSTRACT	18. NUMBER OF PAGES	19a. NAME OF RESPONSIBLE PERSON
UNCLAS	UNCLAS	UNCLAS	SAR		Robert J. Raistrick

19a. NAME OF RESPONSIBLE PERSON: Robert J. Raistrick

19b. TELEPHONE NUMBER (include area code)
781-377-3726

Table of Contents

List of Figures and Tables

Summary

In this final report we summarize research accomplished on the project titled, 'Location, Characterization and Quantification of Hydroacoustic Signals in the Indian Ocean'. Our initial goals were to locate, characterize and quantify hydroacoustic signals recorded on the three available hydroacoustic stations in the Indian Ocean, and this was accomplished for available data through May 2003. However, shortly thereafter our contract was rescoped to focus on high frequency propagation through the convergence zone and blockage. Therefore our work includes results from the 2002 characterization and quantification of observed signals, as well as a detailed analysis of high frequency ice-related signals originating from Antarctica and the blockage of high frequency energy associated with a particularly large earthquake.

In the 'Methods, Assumptions and Procedures' we discuss the analysis methods used in producing the primary results of this project. The 'Results and Discussion' are presented as three sections, the second of which is a near complete draft of a papers about to be submitted to *G-cubed*. The first section is based on work completed prior to the rescope of the work, and is available in more detail as the 2002 catalogue delivered in 2003. The sections therefore contain some repetition of some of the basic analysis methods. The final section (3) of the results and discussions contains recent results from blockage analysis that, along the Section 2 results, were presented at the 2004 Seismic Research Review.

Introduction

Hydroacoustic observations represent a critical component of the global nuclear explosion monitoring effort. They ensure nuclear tests conducted in the ocean, or in the lower atmosphere directly above the ocean, do not go undetected. As such, understanding the nature of background signals, and the underwater propagation of sound within varying conditions, as well as at varying frequencies, helps ensure that signals cannot be easily hidden in certain geographic regions.

Three International Monitoring System (IMS) hydroacoustic stations, Diego Garcia South (H08S), Diego Garcia North (H08N) and Cape Leeuwin (H01W), have been monitoring the Indian Ocean Basin for nearly three years now (Figure 1). Each site has a triad of hydrophones moored ~2 km apart within the SOund Fixing And Ranging (SOFAR) channel, where they record 24-bit acoustic data at a sample rate of 250 Hz. As part of contract DTRA01-01-C-0070, we have characterized and quantified the most commonly observed signal types, as well as the background noise levels, on these three stations during the period January 2002 through May 2003 (Tolstoy and Bohnenstiehl 2002, 2003). Two additional hydrophone triads have recently come online near Crozet Island in the southwestern Indian Ocean (H04N and H04S), but data from these are not discussed here.

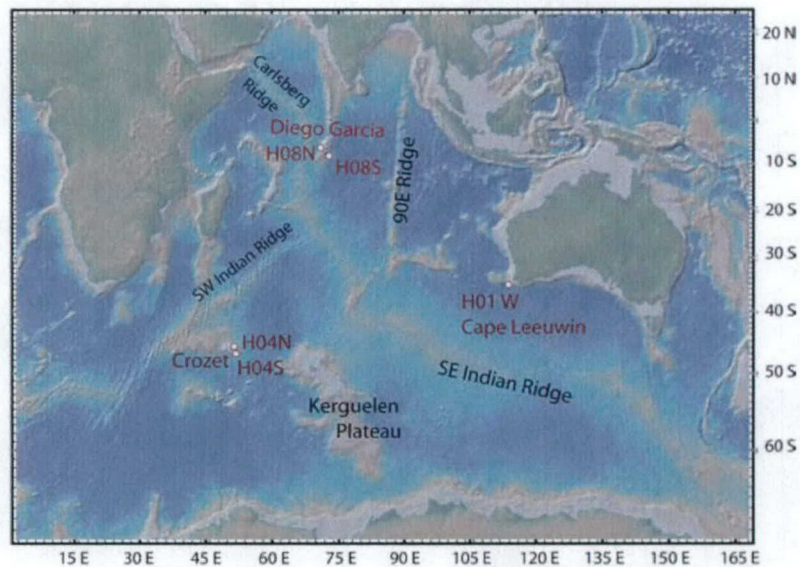**Figure 1.** Location of IMS hydroacoustic stations in the Indian Ocean. Diego Garcia North & South (HO8N & HO8S), Cape Leeuwin (HO1W) and Crozet North & South (H04N & H04S). At each station there is a three hydrophone array, or triad, with an instrument separation of ~2 km. Cape Leeuwin and Diego Garcia have been online since late 2001/early 2002, and data from the Crozet station became available in early 2004.

As part of contract DTRA01-01-C-0070, funding was provided to characterize and quantify hydroacoustic signals in the Indian Ocean. Characterization of all observed signals is important for discrimination so that a signal of concern can be evaluated in context with those typically observed at that site. Such work provides an estimate of the relative importance of each signal, particularly its contribution to the overall background noise at individual stations. As part of this work, annual noise spectra were calculated for each hydrophone site in the Indian Ocean, which assists in understanding detection thresholds for each station at a range of frequencies. Our results for the monitoring of calendar year 2002 have been summarized in the 2002 Annual Catalog (Tolstoy et al., 2003) and the 2003 Annual Report (Tolstoy and Bohnenstiehl, 2003). Results were presented at the 2002 Seismic Research Review (Tolstoy and Bohnenstiehl, 2002). They are summarized in Section 1 of the Results and Discussions.

In June of 2003, the contract was re-scoped to focus on using naturally occurring signals to study blockage of high-frequency energy. One of the exciting results of this contract was the discovery and cataloging of many ice-related signals with significant high-frequency energy (> 30 Hz) (e.g., Tolstoy et al., 2004). While previous work had identified similar ice-related signals within the Ross Sea (Talandier et al. 2002), those signals were recorded at island-based seismic stations with much lower sampling rates. Consequently, it was not possible to detect the energy at higher frequencies or characterize the hydroacoustic amplitudes of the arrivals prior to conversion along the submerged island slope. The origin and frequency content of the observed eastern Antarctic ice noises are discussed in greater detail in Section 2 of the Results and Discussion.

An extremely large (7.6 Mw) earthquake in the northwest Indian Ocean on July 15, 2003 [Bohnenstiehl *et al.*, 2004] has provided very intriguing data with regard to T-wave generation and long-range hydroacoustic propagation. Comparison of arrivals at Diego Garcia North, Diego Garcia South and Cape Leeuwin stations show a strong T-wave arrival at Diego Garcia North, a barely visible lower-frequency T-wave arrival at Diego Garcia South and a strong high-frequency arrival at Cape Leeuwin, despite apparent blockage along the direct path from much of the rupture plane to this station. Travel-time and azimuthal analysis suggests that the earliest T-wave arrival at Cape Leeuwin consists of converted P- and S-wave energy sourced from the eastern scarp of the Chagos and Maldives Archipelagos, at distances of several hundred kilometers from the earthquake rupture. The highest-frequency and highest-amplitude component of the Cape Leeuwin T-wave signal packet exhibits an arrival time consistent with a dominantly hydroacoustic path that may be partially refracted through a bathymetric low to the north of Diego Garcia or represent T-wave energy scattered in the near-field from the region adjacent and to the north of the main rupture. Reflections from bathymetric highs to the north and east of the rupture zone are evident within the T-wave coda. These results are discussed in detail in Section 3 of the Results and Discussion.

Methods, Assumptions and Procedures

Processing Procedures

The data was processed using an interactive IDL-based software package, which has been used successfully to analyze hydroacoustic data within the Pacific, Atlantic and Indian Oceans [Fox et al., 2001]. In order to produce a catalog of events, a dedicated LDEO technician visually inspected all the data available using this software package. The software simultaneously displays the signal amplitude and spectrogram, determined using standard FFT techniques, verses time for all available stations. The time and frequency resolution of the spectrogram display is controlled by varying the FFT window length and overlap. The analyst can make and refine picks using a 0.1-0.5 s scan-line display resolution. The arrival time, acoustic received level and the number/order of hydrophone arrivals are saved to a file. Associated location, source times, acoustic source level and errors, are also saved if a location is possible using three or more stations.

Azimuthal Calculations

Localization of signal source regions can be accomplished using azimuthal calculations, performed for those arrivals with reasonable signal-to-noise ratios (SNRs) at one of the IMS triads. Accurate traveltime differences between each pair of hydrophone channels ($t_{i,j}$) are derived from the cross-correlation of the waveform arrivals and used in a plane wave fitting inversion to determine the horizontal slowness components (p_x, p_y) and estimate the back-azimuth to the source region [e.g., *Del Pezzo and Giudicepietro*, 2002]. This relation between the time delay and horizontal slowness can be expressed as $t = p \cdot \delta$ and solved in a least-squared sense:

$$p = (\delta^T \delta)^{-1} \delta^T t,$$

where X described the geometric position of the hydrophone sensors. The velocity and azimuth are then given as $v = 1/|p|$ and $a = \tan^{-1}(p_x/p_y)$.

Azimuth calculations from stations H01W and H08S, combined with additional ground truth information, have allowed many of the observed ice-related signals to be correlated with specific icebergs, glaciers and ice streams near the Antarctic coast and Eastern Antarctic Ice Shelf (EAIS).

Travel Time Based Location

Differential arrival time data between distant stations also can be used quantitatively to further constrain the source location of the signals. For a simple uniform velocity medium, the travel time t_i to a station i is simply given as $t_i = d_i/v$, where d_i is the distance from the source location to the station location. Given a differential arrival time of ΔT sec between the arrival of a signal at two stations (*i and j*), the source location can be constrained along a line whose points (x, y) satisfy the relationship (**5.2.1** IDC Processing of Seismic, Hydroacoustic, and Infrasonic Data):

$$\Delta T = (d_i - d_j)/v$$

For instances, observations using available IMS data from the Indian Ocean (2002-2003) have shown that ice-related tremor signals typically arrive at the H08S station with a 45-55 minute delay relative to those at H01W (arrivals at H08N are largely blocked by the shallow atoll). Source locations can be determined using a grid-search implementation (3 x 3 km node spacing) and are discussed further in Section 2.

RESULTS AND DISCUSSION - SECTION 1

Characterization and quantification of hydroacoustic signals in the Indian Ocean

M. Tolstoy, D. Bohnenstiehl, and E. Chapp

ABSTRACT

Data from three International Monitoring System hydroacoustic stations in the Indian Ocean (Diego Garcia North, Diego Garcia South, and Cape Leeuwin) have been analyzed for the calendar year 2002. These stations provide real-time hydroacoustic data and were designed to monitor for covert nuclear testing. It is important to characterize noise and commonly observed signals in the ocean to better understand detection levels, source discrimination and contributions to global ocean noise budget. Hydroacoustic signals also provide a wealth of scientific data on topics as diverse as ocean crust evolution to marine mammal migration. Analysis of the 2002 Indian Ocean data includes characterization and quantification of observed signals as well as determination of seasonal background noise variations. The hydroacoustic stations allow signals in the 1-125 Hz range to be observed, with the system response flat within ~3 dB from 5-100 Hz. These include earthquake phases, iceberg related noise, shipping, marine mammals, and seismic surveys. We show that the temporally dominant signals include anthropogenic noise (primarily shipping) and marine mammals. Individual picked signals are dominated by earthquakes and noises related to ice-movement. Background noise levels vary seasonally and can be tied to weather, marine mammal migration, anthropogenic activity and possibly ice movement in Antarctica.

INTRODUCTION

Land based monitoring of earthquakes can be traced back many centuries and enormous scientific effort has been put into understanding the signals that seismographs record. In comparison, hydroacoustic monitoring of the oceans is a very recent development, and the water bourn T-wave phases of an earthquake were only defined in the early 1950's (Tolstoy & Ewing, 1950). The SOFAR (SOund Fixing And Ranging) channel in the ocean provides an efficient low-velocity waveguide that can trap sound energy and transport it great distances with relatively little loss in signal strength. This makes hydroacoustic monitoring a powerful tool for detecting small acoustic signals originating in the ocean or along its seafloor and sea surface interfaces.

International Monitoring System (IMS) hydroacoustic stations in the Indian Ocean are designed to detect and help locate any covert nuclear tests in the ocean basin. In order to efficiently utilize hydrophones for explosion monitoring, it is important to have the 'typical' sounds observed well characterized. In this way signals of concern can be compared to what is already known. Background noise levels of the stations, which can vary seasonally, are also important to characterize since this will impact the event magnitude that the station is able to observe. To this end, we have characterized and quantified signals observed and background noise in the Indian Ocean for 2002.

Contributions to the noise budget of the Indian Ocean including continuous sources such as wave and wind noise, as well as transient and impulsive signals that are can be biological, geological or anthropogenic in nature. Quantifying the global ocean noise budget is a goal of increasing attention (NRC Report, 2003), with particular emphasis on how recent increases in anthropogenic noise may impact marine mammals in an already stressed ocean environment. Here we quantify the ocean noise budget in the low frequency ~5-100 Hz range.

Whales are believed to use the SOFAR channel to communicate, and the calls of several species of baleen whales can be observed regularly. Shipping is by far the most commonly observed anthropogenic signal, and earthquakes and sounds related to ice movement are the most common geological sources.

DATA

Hydroacoustic data from three IMS stations in the Indian Ocean (Figure 1-1) have been analyzed for all days available in 2002. These stations, Diego Garcia South (H08-S),Diego Garcia North (H08-N) and Cape Leeuwin (H01-W) each have a triad of hydrophones moored ~ 2 km apart within the SOFAR channel, recording acoustic data at a sample rate of 250Hz. The system response of the IMS hydrophones is flat to within ~3 dB between ~5-100 Hz, although some additional information is preserved within the 100-125 Hz and 1-5 Hz range. For each station only one channel was used for picking events, since the close spacing of the phones means that signals look essentially the same on all 3 channels. However, the stations can be used for estimating the azimuth from the hydrophone array to the signal source, which has proven useful in source identification.
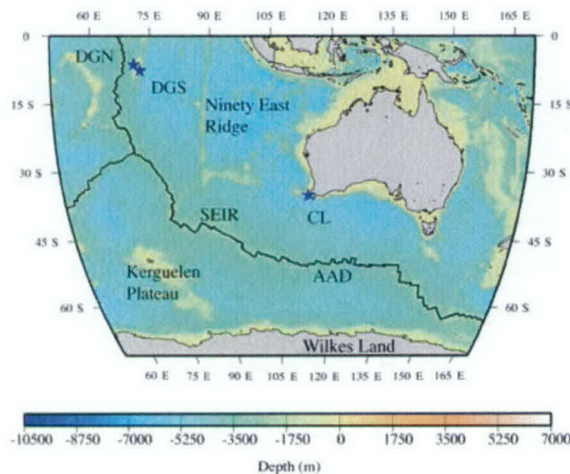
Figure 1-1. Map of Indian Ocean Basin study area. Blue stars indicate hydrophone triad locations labeled as CL (Cape Leeuwin), DGS (Diego Garcia South) and DGN (Diego Garcia North. Mid-ocean ridges shown as black lines with the following geographic location labels: Southeast Indian Ridge (SEIR), Australian-Antarctic Discordance (AAD), Ninety East Ridge, Kerguelen Plateau, Wilkes Land section of Antarctica. Color bar indicates sea floor bathymetry in meters relative to sea level.

There were some days in 2002 during which there was either no data or unreadable data in the files supplied by the Center for Monitoring Research (CMR), which was the organization charged with distributing IMS data to those with Defense Threat Reduction Agency (DTRA) contracts to use the data. The data gaps are summarized in Table 1-1, and indicated on histograms.

Station	Cape Leeuwin	Diego Garcia South	Diego Garcia North
	001-006	001-022	001-021
	057	057	057
	064	064	064
	123-124	123-124	123-124
	136	136	136
	234	172	180-189
	244	180-190	234
	314	234	244
	324	244	324
	336	311	336
	346	324	355
	355	336	
	359-365	355	
Total Days Missing	**25**	**45**	**41**

Table 1-1: Data gaps for 2002 on Indian Ocean hydrophone sites.

BACKGROUND NOISE CHARACTERISTICS

The background noise at the three operational hydrophone stations has been characterized for all available days of 2002. Noise levels at hydrophone sites are controlled by a number of factors including proximity to shore (wave noise), weather variations and shipping in the area. The level of background noise is a critical factor in the ability of a station to observe specific events. As background noise increases, the detection sensitivity of the station decreases accordingly. As discussed below, many noise sources are seasonal; therefore, it is important to characterize the noise for the full annual spectrum.

In general Diego Garcia North is quieter than Diego Garcia South, and both are quieter than Cape Leeuwin (Figures 1-2, 1-3 and 1-4). However, daily noise variations at each station are substantial. In addition, variations in noise levels are highly frequency dependent.

Cape Leeuwin - Annual Variations

Figure 1-2a shows monthly averages of power spectral density at Cape Leeuwin for 2002, and figure 1-2b shows quantiles for daily variations. Power spectral density (PSD) information was derived from daily Pwelch averages, using zero-padded Hanning windows with a length of 30 minutes. These daily PSD curves were then smoothed by averaging over 0.25 Hz frequency bins. Empirical quantile values were derived from the distribution of PSD values in each frequency bin. In the ~5-15 Hz range there is a seasonal variability with noise levels being highest from January-June, possibly due to changes associated with increased ice movement or potentially weather related.

Figure 1-2 A – Monthly averages of power spectral density estimate for Cape Leeuwin. B. – Empirical quantile values were derived from daily power spectral estimates for calendar year 2002.

Figure 1-3 A – Monthly averages of power spectral density estimate for Diego Garcia South. B. – Empirical quantile values were derived from daily power spectral estimates for calendar year 2002.
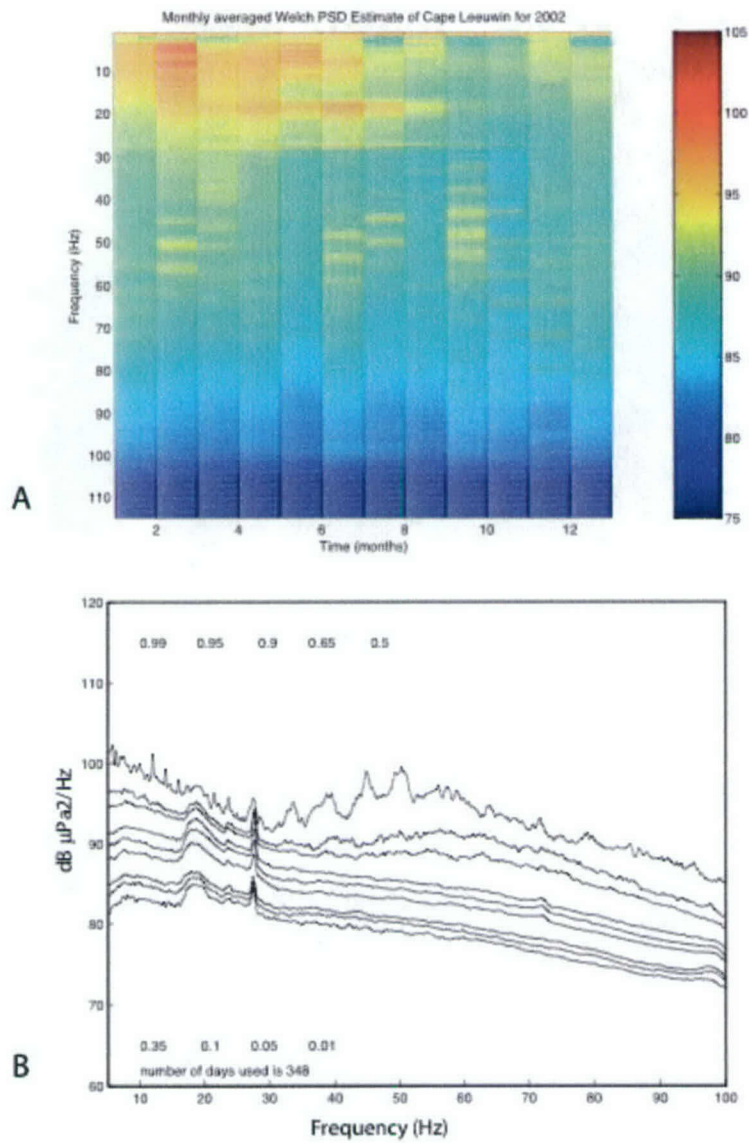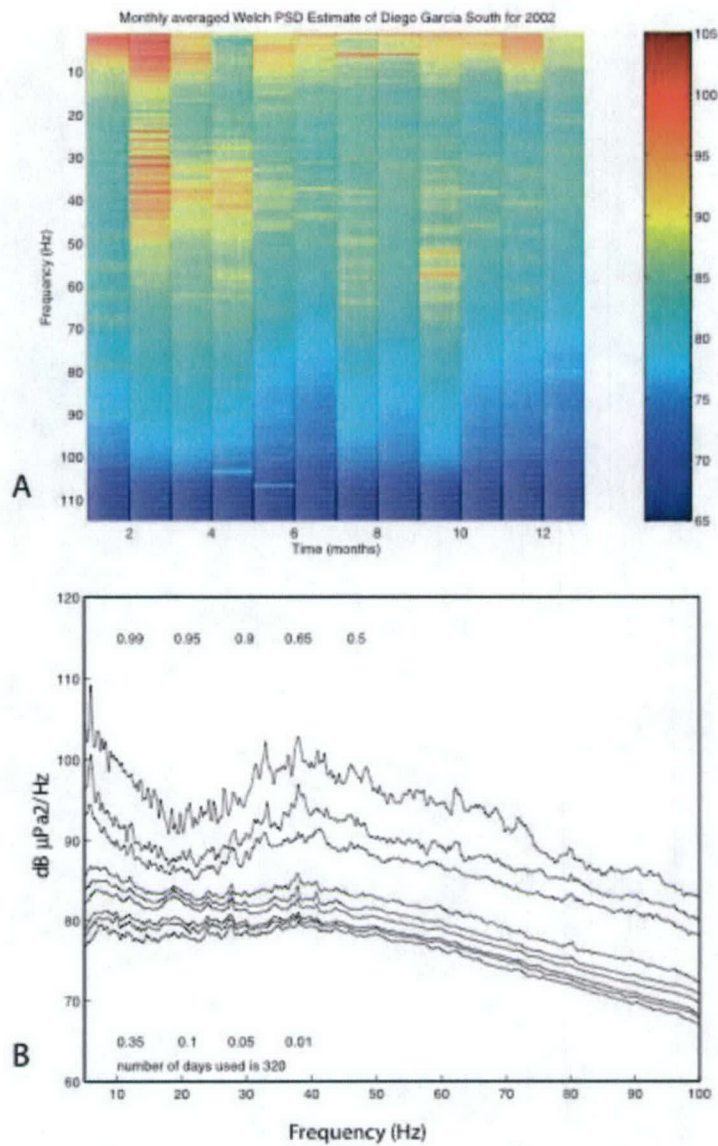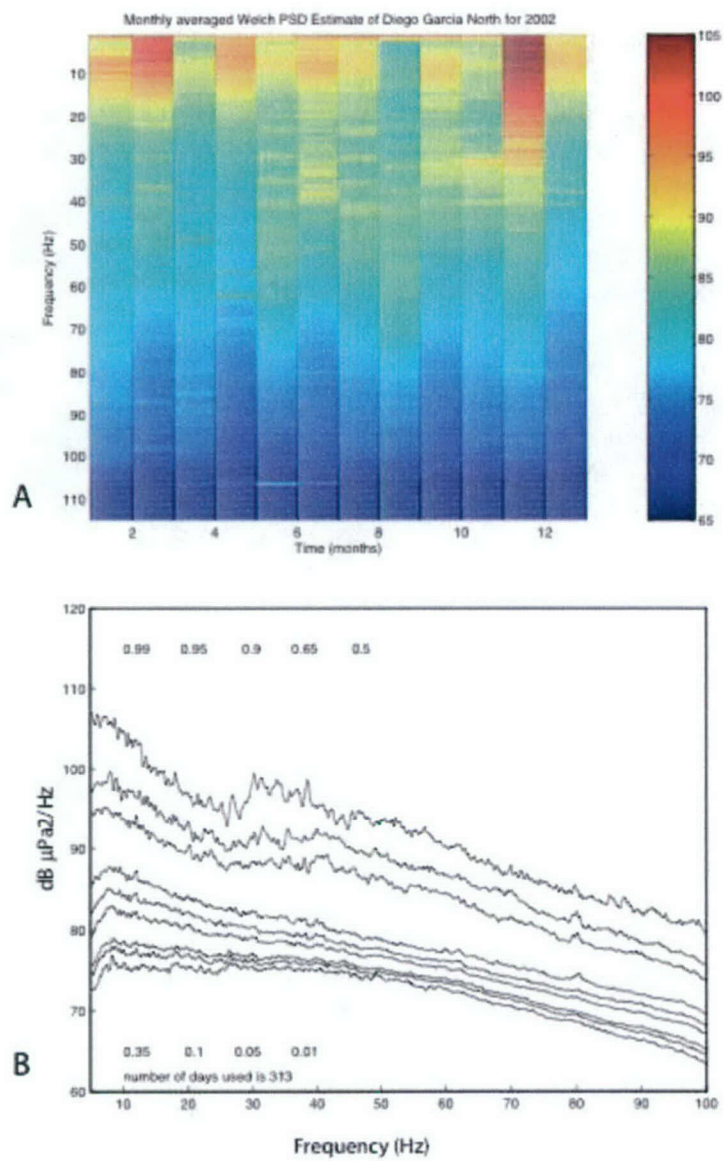
Figure 1-4 A – Monthly averages of power spectral density estimate for Diego Garcia North. B. – Empirical quantile values were derived from daily power spectral estimates for calendar year 2002.

Particularly notable are peaks in the spectra in the ~18-28Hz range with a broad bump noticeable at the low end of the range and a spike like increase around 28Hz. This noise band peaks in the Austral winter and is most likely due to increased levels of whales calls (Curtis et al., 1999) associated with seasonal migrations, particularly the Antarctic Blue, which migrates through the area over that time (Stafford et al. 2004), but may also have contributions from strumming of the hydrophone cable as the weather deteriorates as well as increased wave noise (McCreery et al., 1993). At frequencies greater than 50 Hz, differences drop to just a few dB, with the largest variations coming from harmonic peaks that are likely associated with passing ships.

Figure 1-2b shows the daily noise power spectral density values for Cape Leeuwin, with red lines showing various quantile levels for daily averaged spectra. The figure shows a ~10-15 dB re 1µPa variation in the 5% and 95 % levels across the full range of frequencies, illustrating that noise levels can vary significantly on an annual and daily basis. Daily variations can be as high as 30 dB re 1µPa in both low frequencies (<15 Hz), and the mid range 40-60 Hz frequencies, likely due to particularly large earthquakes (or explosions) and ships, respectively.

Diego Garcia South - Annual Variations
Noise variations at Diego Garcia South are dominated by ship noise since the site is relatively close to the main harbor entrance of Diego Garcia, which is a naval base (Figure 1-3). Low-frequency energy is notably high in February and November, associated with what appeared to be a series of explosions to the north of Diego Garcia, which are interpreted to be naval exercises (see Diego Garcia North). The fact that relatively few days of data were available in January for this station makes the average monthly noise levels for January potentially less representative. A small noise spike can occasionally be seen at ~110Hz, attributed to a whale call, but it is not as pronounced as on Diego Garcia North (see below). Cyclones are apparent in the very low frequency band for daily and weekly averages (not shown).

Figure 1-3b shows the daily noise power spectral density values for Diego Garcia South with red lines showing various quantile levels for daily averaged spectra. The figure shows up to 20 dB variation in the 5% and 95 % levels particularly in the lower frequencies (~5 Hz), and in the 30-50 Hz range, which is dominated by ship noise. This illustrates that noise levels can vary significantly on an annual and daily basis. Daily variations can be higher than 30 dB in both low frequencies (~5 Hz), and the mid range 25-60 Hz frequencies, likely due to earthquakes/explosions and ship noise, respectively.

Diego Garcia North - Annual Variations
Noise variations at Diego Garcia North are similar to those at Diego Garcia North, which is not surprising given their relative proximity (Figure 1-4). However, there is less pronounced shipping noise, likely because DGN is further from the harbor entrance and on the opposite side of the island. However, the series of explosions that were apparent in the DGS spectrum, dominate the February and in particular the November monthly averages. Also notable is a seasonal appearance of a spike at ~110 Hz, (note the data is

band-pass filtered at 100 Hz, so values shown are lower than true values), due to a 110 Hz whale call that was frequently seen in the area (see below).

Figure 1-4b shows the daily noise power spectral density values for Diego Garcia North with red lines showing various quantile levels for daily averaged spectra. The figure shows up to 25 dB variation in the 5% and 95 % levels particularly in the lower frequencies (~5-10 Hz) due to particularly high noise levels associated with explosions. Variations are lower than DGS and in the 30-50 Hz range, which is dominated by ship noise, with ~15 dB variation in the 5% and 95 % levels. Daily averages varied by almost 50 dB at the lowest frequencies, again attributed to probably explosions nearby the station.

SIGNAL CHARACTERIZATION AND QUANTIFICATION

Hydroacoustic data have been used extensively over the last decade to study geological processes (e.g. Fox and Dziak, 1998; Fox et al. 2001) and marine mammal calling and migration patterns (e.g. Stafford et al., 2004). In addition, land-based stations have been used to identify signals related to ice movement that travel through the SOFAR channel and are converted on island slopes to seismically recordable phases (e.g. Okal et al., 2002; Talandier et al., 2002). Here we build on this previous work to quantify known signals, and characterize, identify and quantify unknown signals.

All data (one channel from each hydrophone channel) was visually inspected using IDL-based software developed by C. Fox and others (Fox et al. 2001) specifically for analyzing hydroacoustic data. The data is scrolled through time with both waveform and spectrograms being displayed side by side. The spectrograms are the most useful feature for signal identification, and allow relatively small but distinct signals to be recognized that might otherwise be unidentifiable in the noise of simple waveform data. Characterization was based on the spectral character of the signal, sometimes combined with azimuthal estimates to help identify possible source locations.

All arrivals were hand picked (as opposed to automatic picks which can provide many false picks as well as missing numerous signals). Individual non-impulsive signals such as T-waves or bloops were picked at their peak energy, and impulsive arrivals such as P-waves were picked at the beginning of the arrival. For frequently occurring and repeating signals where arrival times were not critical, the arrivals were categorized per hour. So individual hours were flagged as containing that signal, and hence a maximum of 24 observations could be made per day. This simplified the cataloging of repeating sources such as airguns or whales, and signals that were not impulsive such as ship noise. For other individual impulsive signals, such as earthquake arrivals, the each event was picked (and counted) individually.

The observed signals are therefore classified as 'hourly' signals (e.g. whales, ship noise, airguns, and pulsed iceberg tremor series (cusped pulsed tremor)), and 'picked' signals (e.g. earthquakes, prolonged iceberg signals (variable harmonic tremor), sharp signals, and bloops). These signals are discussed in five categories specific to their origin: Geological (earthquakes), Anthropogenic (e.g. ship noise); Biological (e.g. whales);

Icebergs; and Other (e.g. unknowns). Spectrograms and histograms for all these signals are available in the previously delivered 2002 catalogue.

GEOLOGICAL:

T-waves

The most common geological signal is the T-wave, which is the water bourn phase of an earthquake that travels in the SOFAR channel. The strength of the T-wave is related to the magnitude of the earthquake as well as the topographic character of the source area. For instance a rough seafloor scatters energy more efficiently into the SOFAR channel and results in a stronger T-wave signal compared with a sedimented area. Similarly, a sloped surface is a more efficient transmitter of this horizontally traveling energy than a flat surface. In the Indian Ocean the primary source of T-waves is the mid-ocean ridge system, which spans the basin to the southwest, southeast and north. While considerable seismicity is generated in the Java-Sumatra trench, much of this does not produce T-wave energy since the sources are quite deep, and do not have an easy path into the SOFAR channel.

T-waves are emergent arrivals, with a peak energy arrival and coda. Arrivals times are picked on the peak energy time. T-wave occurrences are distributed fairly continuously throughout the year with no apparent seasonal trend. This suggests that seasonal noise variations at the different sites are not large enough to significantly reduce the magnitude of completeness. However, this should be verified through seasonal magnitude of completeness calculations, since a few large events and their aftershocks could mask seasonal variations if looked at purely in terms of absolute number of events. Peaks in the histograms are generally associated with a large mainshock event followed by a series of aftershocks. In one case earthquakes associated with a probable volcanic swarm were observed on the Southeast Indian Ridge.

Note that numerous other seismic phases can be identified in the record when a large enough earthquake occurs. However, these would be well known from the global seismic network, and so could be eliminated as sources of concern. The most frequent of these phases is the P-wave arrival, which is discussed below. P-waves have visual characteristics similar to an explosion, but can be distinguished through cepstrum analysis that will indicate bubble pulse peaks if the source is an explosion, as discussed below.

ANTHROPOGENIC:

Airguns

Airguns create sharp impulsive signals that are easily distinguished by their shape and their evenly spaced repetitive nature. Airgun surveys are conducted primarily by oil companies exploring for new oil fields, and also by academic researchers mapping geological structure. Note that airgun energy can travel thousands of kilometers if the shooting is occurring in an area conducive to scattering into the SOFAR channel. There are some obvious seasonal patterns in the shooting, with limited shooting in the Austral winter at Cape Leeuwin, as well as during monsoon season at Diego Garcia North.

Ship noise
Ships tend to produce monochromatic bands that gradually fade in, become stronger, and then fade out. The frequency of these bands and/or mechanical noises associated with the ship is dependent on the type of ship and specifically the engine and propulsion system. Both Diego Garcia sites and the Cape Leeuwin site are close to busy shipping areas, so there is considerable shipping noise apparent at all three locations. Shipping noise is therefore fairly continuous at both sites, with perhaps a slight drop off observed at Diego Garcia North during monsoon season, and a slight dip during the Austral winter at Cape Leeuwin. However, in general shipping noise was observed for some period every day at every site.

Possible Explosions /P-waves
However, large events generated outside of the ocean basin produce P-waves with no accompanying T-wave to clearly distinguish it as a seismic arrival, and regional events can have a significant time gap between the P-wave and T-wave making them harder to associate. In this case the P-waves can be distinguish either through correlation with an earthquake cataloged in the REB or through cepstrum analysis that would not show a bubble pulse. For the purposes of this work we were not routinely performing cepstrum analysis, and so potential explosions and solitary P-waves were not always distinguished in the picking process. However, we believe that the majority of them were P-waves. There are numerous regional events near Diego Garcia that generate observable P-waves; however, we have identified several days in November and February when we believe significant explosions took place near Diego Garcia North, likely as part of an exercise.

BIOLOGICAL:
The primary biological signals observed on the hydrophones are whale calls. There are only a few species of whales that are known to make sounds in the 1-125 Hz range of the hydrophones. These are minke, fin and blue whales. In general very little is know about whale song globally and even less in the Indian Ocean, which to date has not been a focused site for whale monitoring. So many of the calls identified here have not been seen elsewhere, or are similar, but not quite the same as calls observed in the Pacific or Atlantic oceans (Stafford et al., 2004, personal communication).

Minke Whales
Minke whale calls exhibit pulses that come in small packets with relatively even spacing between the individual pulses to form a pulse train and minutes between packets of pulse trains. The seasonal pattern is quite striking and similar at all three stations, with a clear bias toward the latter half of the year. All three sites show virtually no calls in the first half of the year (though the large data gaps in January may mean that some 'leakage' into that month would not be observed at the Diego Garcia sites). Note there are two hours in January during which calls are observed at Cape Leeuwin. However minke whale observations at both Diego Garcia sites do appear to have ended prior to the end of December. Both Diego Garcia sites show calls starting in mid June and peaking around the end of September, with calls abundant from mid-August through the mid-November. The fact that the peaks are somewhat more defined at Diego Garcia relative to Cape Leeuwin, may indicate a migratory pattern north in the Austral spring (Sept.-Nov.) It is

possible that the Indian Ocean minke whales spend the Austral summer and fall feeding in the Antarctic waters, and therefore are not observed during this period (January-May) at further north areas such as Cape Leeuwin and Diego Garcia.

Fin Whales

Fin whale calls exhibit short sharp repetitive pulses around 20Hz. Fin whale calls also indicate a seasonal pattern similar to that of the Minke whale, with calls only being observed in the latter half of the year. Again this suggests a possible feeding period in Antarctic waters in the first half of the year, with a migration north for the latter part of the year.

Blue Whales

Numerous different types of calls were observed that have previously been characterized as blue whales. There were a number of calls that were identified as likely whale calls, but for which no clear classification could be found in the literature or from talking with whale call experts. However, the low frequency of the calls makes it quite likely that they are an as yet unidentified blue whale call. Most show seasonal trends, but the timing of these trends is quite variable. For instance some whales appear primarily in the early part of the year. A few were seen only on the Cape Leeuwin station or the Diego Garcia stations.

OTHER:

Sharp signals

One unidentified signal was referred to as a 'sharp signals'. It appears similar to an airgun signal, spike like in nature across the full range of observable frequencies, but it does not appear to be airgunning because the signals do not continue in time or show any clear relation to the airgun surveys that are observed. It does not exhibit a bubble pulse (in cepstrum analysis), and so is not likely to be an explosion. It has been suggested that it may be associated with ice movement in Antarctica. The signal appears fairly consistently throughout the year at Cape Leeuwin and Diego Garcia south, but less consistently at Diego Garcia North where it is quite rare in the Austral Winter-Early Spring time frame (June-Oct.). This is consistent with the signal being ice-related, since only the stronger signals would be likely to reach Diego Garcia North with a less clear path to the ice-sheets, and ice movement is less common in the Austral winter period.

Ice-generated tremor

As discussed in detail in Section 2 of this report, there are a number of different signals generated by the movement of ice-sheets and icebergs in Antarctica.

Bloops

Another unidentified signal has been termed a 'bloop'. It is a signal with energy in the 1-50 Hz range, with a sweeping up of the most pronounced frequency through time. There is a clear seasonal bias for the Austral summer and fall, and the azimuths for these signals indicate an origin near coastal Antarctica, though there were few good azimuths obtained. The signals therefore might be interpreted as being related to the summer break-up and movement of ice in that area.

SUMMARY
Figure 1-5 shows pie charts indicating the relative abundance of both picked and hourly
signals at each station. The dominant signal varies from station to station quite notably.
For Diego Garcia North the picked signals are dominated by T-waves, with a significant
number of P-waves and possible explosions. Because explosions look quite similar in
character to P-waves, they were categorized together. To distinguish between the two,
cepstrum analysis needs to be done to identify the presence of a cepstrum peak (if the
signal is from an explosion). It is thought that the majority of the picks in 2002 were P-
waves (see 2002 annual catalogue for discussion and examples). There are numerous
regional events near Diego Garcia that generate observable P-waves; however, we have
identified several days, particularly around the time period around Julian day 350, 2002
when a series of events were observed in the vicinity of Diego Garcia that we believe to
be explosions.

Also observable at Diego Garcia North were a small number of ice-related signals,
although the position of the station on the North side of the island means that the vast
majority of these signals, coming from Antarctica, are blocked. The few signals that are
observed tend to be in the 'unknown' category such as 'bloops' and 'sharp signals' that
are thought to be ice-related, but have not definitively be shown to be so.

Hourly signals at Diego Garcia North were dominated by whales calls, followed by ship
noise. In particular, a 110 Hz blue-whale call was so frequent that it would sometimes
cause a spike in the monthly spectrum (see April in Figure 1-3 and 1-4). There is also a
small, but significant amount of airgunning observed. Airgun activity, primarily from oil
industry exploration ships, can be quite dominant when it is occurring, with 10-20 second
intervals between impulsive broadband arrivals.

For picked arrivals at Diego Garcia South, T-waves were again the most frequently
observed signal, but with ice-related signals following as a close second. There were
significantly fewer P-wave/explosions observed. Hourly signals were again dominated by
ship noise and whale calls, with slightly higher ship noise than whale calls. Again, there
is a small but significant amount of airgunning observed, as well as a tiny amount of ice-
related noise. For the hourly signals, ice-related noise was cusped harmonic tremor
associated with ice-stream movement on the coast of Antarctica.

For Cape Leeuwin picked arrivals, ice-related signals are by far the dominant arrival,
reflecting the stations proximity and clear path to Antarctica. There were significantly
fewer T-waves observed than at the Diego Garcia station, likely reflecting both the higher
background noise levels, and the perhaps fewer earthquake source areas with direct paths
to the stations. There were just a few P-wave/explosions observed at Cape Leeuwin
probably due to the high background noise levels and low level of regional seismicity.
For hourly signals at Cape Leeuwin ship noise was by far the most dominant signal, with
smaller but significant whale call activity and airgunning. There is also a small, (but
significantly larger than Diego Garcia stations), amount of ice-related signals, again
related to ice-stream movement on the coast of Antarctica.

DIEGO GARCIA NORTH   **DIEGO GARCIA SOUTH**   **CAPE LEEUWIN**

PICKED SIGNALS

Ice Related

T-waves

P-waves/
Explosions

(Total Picks = 9108)

Ice Related   T-waves

P-waves/Explosions

(Total Picks =8035)

T-waves

P-waves/
Explosions

Ice Related

(Total Picks = 12434)

HOURLY SIGNALS

Aiguns

Whales

Ship

(Total Hours = 14907)

Airguns

Whales

Ship

Ice Related

(Total Hours = 15324)

Airguns

Whales

Ship

Ice Related

(Total Hours = 10114)

DIEGO GARCIA NORTH   **DIEGO GARCIA SOUTH**   **CAPE LEEUWIN**

Figure 1-5. Top pie charts show relative number of picks for different signals at stations Diego Garcia North, Diego Garcia South and Cape Leeuwin. This chart includes all signals for which individual arrival times were picked. Ice-related signals for picked events included iceberg movements, bloops and sharp signals, all believed to be related to ice movement in Antarctica. Total number of picks for all signals at each station is given below the pie chart. Bottom pie charts show relative number of hours for different signals recorded at all three stations. This chart includes all signals that were assigned hourly values - i.e. where an hour was marked as having the signal present or not present. The ice related signal is harmonic tremor associated primarily with ice-stream movement in Antarctica. Total number of hours of all signals at each station is given below the pie chart. Note, that since some hours contained more than one signal type, there are potentially more than 24 hours picked per day.

SECTION 2

Sound-Channel Observations of Ice-Generated Tremor in the Indian Ocean

Emily Chapp[*], DelWayne R. Bohnenstiehl and Maya Tolstoy

Lamont-Doherty Earth Observatory of Columbia University, P.O. Box 1000, Palisades,

NY 10964, USA

Abstract. Mid-to-low latitude hydrophone stations within the Indian Ocean have recorded two distinct types of low-frequency (<100 Hz) tremor that can be correlated with drifting icebergs and glacial features along the Wilkesland coast of eastern Antarctica. The most common of these signals is a variable harmonic tremor (VHT), with spectral peaks that exhibit frequency fluctuations through time. These signals typically display a 4-10 Hz fundamental frequency and may have as many as eight harmonic bands. Individual VHT signal packets have durations of up to ~30 minutes and occur throughout the year in clusters that continue for hours-to-days. A second, less-commonly observed signal is characterized by shorter duration (25-60 sec) pulses with a convex-upward spectrogram appearance. These cusped pulse tremors (CPT) often exhibit a near uniform pulse spacing, with episodes continuing for minutes-to-hours. Tremor received levels at hydrophones near 32° S, 114° E and 7° S, 72° E reach as high as 142 and 133 dB re 1 μPa (peak-to-peak), respectively. Propagation likely occurs as a sea surface-reflected phase at high latitudes and sound channel phase north of the convergence zone, with low-frequency transmission loss estimates suggesting maximum acoustic source levels of ~245 dB re 1μPa @ 1m. Source locations for a subset of the loudest VHT signals correlate with the satellite-derived locations of a large iceberg (B-15D) that migrated westward along the Wilkesland shelf region during 2002 and early 2003. Most VHT signals, however, cannot be correlated with named icebergs, suggesting that these signals also may be sourced from smaller unnamed icebergs and/or outlet glaciers distributed along or near the Wilkesland coast. CPT signals have a more limited spatial distribution, originating from five specific regions where active ice stream activity is observed. The harmonic nature of both signal types is consistent with the resonance of an ice layer or fluid-filled cavity within an ice mass.

1. Introduction

Numerous submarine volcanic eruptions have produced tremor signals that were

coupled efficiently into the ocean's low velocity sound channel [e.g., Talandier and Okal,

[*]Now at School of Ocean and Earth Science and Technology, University of Hawaii, 1680 East-West Road, Honolulu, HI 96815, USA

19

1987; Dziak and Fox, 2002]. Both island-based seismic stations and moored hydrophones have recorded these signals, which exhibit a diverse suite of broadband, monochromatic and polychromatic spectral properties. In late 2000, island-based seismic stations belonging to the Polynesian Seismic Network (PSN) recorded ice-generated noises associated with drifting icebergs within the Ross Sea [Talandier et al., 2002]. The spectral characteristics of these signals resembled those of previously identified volcanic tremor, exhibiting a 4-7 Hz fundamental frequency with multiple overtones; however, the spatial and temporal distribution of the signals correlated closely with recently calved and drifting icebergs. Talandier et al. [2002] proposed that the source of these tremors was the resonance of the iceberg or a fluid filled cavity within the ice mass. As the signals were only recorded when the iceberg remained on the shallow bathymetric shelf, they suggested that excitation of the resonator was driven by the scraping of the iceberg across the seafloor.

Three International Monitoring System (IMS) hydroacoustic stations, Diego Garcia North (DGN), Diego Garcia South (DGS) and Cape Leeuwin (CL), have been monitoring the Indian Ocean Basin since the beginning of 2002 (Figure 2-1). Each site has a triad of hydrophones moored ~2 km apart and floated within the SOund Fixing And Ranging (SOFAR) channel. Analysis of these data has identified reoccurring ice-generated tremor signals at both the CL and the DGS hydrophone stations, which provide unblocked paths to the Wilkesland section of the eastern Antarctic coast (85° E - 149° E longitude). Location analysis of the tremor signals and available ground-truth information provided by satellite imagery suggests these signals may be associated with a diverse set of environments—including drifting icebergs, outlet glaciers and ice streams.

20

With respect to spectral content and duration, these signals are the most diverse

hydroacoustic arrivals observed within the 1-100 Hz frequency range for the Indian

Ocean, and their prevalence may make them a significant contributor to the ambient noise

within the basin. Below we characterize their signal properties and describe their spatial

and temporal associations with Antarctic ice. Relative to previous observations using

island-based seismometers [e.g., Talandier et al., 2002], IMS hydrophone-based

observations allow for characterization at somewhat higher frequencies of up to 100 Hz.

Moreover, the location of the IMS sensors within the oceanic water column avoids the

complexity associated with acoustic-to-seismic conversion along a submerged island

slope [e.g., Talandier and Okal, 1998] and allows us to better constrain the acoustic

source levels of these signals.

2.0. Signal Detection and Identification

IMS hydrophone stations DGN (6.3°S, 71.0°E), DGS (7.6°S, 72.5°E) and CL

(34.9°S, 114.1°E) were deployed in support of the Comprehensive Test Ban Treaty and

designed to detect the sounds generated by explosions that may be carried out at or below

the ocean surface. The data used in this study were made available in support of a

broader project of Indian Ocean noise characterization, under contract from the Defense

Threat Reduction Agency. The northern two stations DGN and DGS are located ~180 km

to the northwest and ~25 km to the south of the Diego Garcia island atoll, respectively.

The CL station is located ~100 km to the southwest of the Australian coast (Figure 2-1).

The stations consist of three hydrophones deployed in a triangular configuration (triads)

with approximately 2 km spacing between instruments. Hydrophone sensors are moored

to the seafloor and floated near the sound channel axis, where they record continuously at

a sample rate of 250 Hz and 24-bit A/D resolution. The system response is flat to within 3 dB over the frequency range ~3-100 Hz.

Hydrophone data were inspected visually using a software interface originally developed for the analysis of regional hydrophone array data [Fox et al., 2001]. This software displays both signal traces and spectrograms, which can be scrolled through time. The occurrence of tremor signals was flagged by an analyst, with the arrival times, station name and descriptive comments saved. Available data between January 2002 and May 2003 are examined in this study.

Tremor was observed to be most prevalent and exhibited the largest amplitude at the most southerly station CL. Tremor signals with the loudest received levels at CL could also be identified at station DGS, where they arrived with a relative delay of 35-50 minutes—suggesting a source region within the southern Indian Ocean. These signals could not be clearly identified at station DGN, as the shallow bathymetry of the Diego Garcia atoll blocks hydroacoustic paths along many southern azimuths. Unless otherwise noted, the received levels of the tremor signals are characterized using the maximum peak-to-peak amplitude within the signal packet, reported in decibels (dB) relative to a reference value of 1 μPa.

3.0. Location Analysis

3.1. Azimuthal Constraints from Hydrophone Triads

To localize the source regions of the hydroacoustic tremor, travel time differences between each pair of hydrophones ($t_{i,j}$) within a station's triad were derived from the cross-correlation of the signal arrivals. These delay times were used in a plane wave fitting inversion to determine the horizontal slowness components (p_x, p_y) and estimate

the back-azimuth to the source region [e.g., Del Pezzo and Giudicepietro, 2002]. This

relation between the time delay and horizontal slowness can be expressed as the dot

product $t = p \cdot \delta$ and solved in a least-squared sense:

$$p = (\delta^T \delta)^{-1} \delta^T t \qquad (1),$$

where X describes the geometric position of the hydrophone sensors. The velocity (v)

and azimuth (α) are then given as $v = 1/|p|$ and $\alpha = \tan^{-1}(p_x/p_y)$.

As the sound velocity in the vicinity of the mid-to-low latitude arrays is

reasonable well constrained, the slowness value returned by the inversion, along with the

correlation coefficient between instruments, can be used to assess the quality of the

azimuthal estimates. To quantify the error in these azimuthal calculations, well-located

earthquakes at distances of 130-3500 km were used as references sources [e.g., Hanson

and Givens, 1998]. The angular differences between the estimated and predicted

azimuths of these plane wave arrivals were computed using a suite of 27 signals at DGS

and 34 signals at CL. The standard deviations of the misfits are 1.51° and 1.26° at the

respective stations. These errors are taken to represent the 1-σ limits in our azimuthal

calculations.

3.2. Differential Travel Time Constraints

The absolute arrival time information from the two stations, DGS and CL, are

insufficient to invert for the location and origin time of the tremor signals; however, the

set of all possible source locations that satisfy the observed arrival-time differences (ΔT)

between these stations can be defined. In the simplest case of a uniform propagation

medium with constant velocity (v), the differential arrival time between the stations is

given by the following relationship:

$$\Delta T = \frac{d_{DGS}}{v} - \frac{d_{CL}}{v} \qquad (2),$$

where d_{DGS} and d_{CL} are the distance between the source location and the receiving

hydrophones.

To validate the locations determined by the azimuthal crossings (Sect. 3.1), the

points satisfying Eq. (2) were found with a grid search method using a 3-by-3 km node

spacing. For each arrival time pair, this generated a curve along which the same ΔT

values are predicted due to the trade off between location and origin time. Assuming a

propagation velocity of 1.475 km/s, a reasonable average for a signal whose path

originates south of the convergence zone, resulted in the best overall consistency between

the azimuthal locations and the ΔT curves, with each of these curves passing through the

error field of the azimuthally derived location. Note that as not all signals are well

recorded on the more distant DGS station, these methods can only be used to locate a

subset of the signals observed.

4.0. Variable Harmonic Tremor (VHT) Observations

4.1. VHT Signal Characterization

The dominant tremor type observed at the DGS and CL stations consists of

multiple harmonic bands with spectral peaks that fluctuate in frequency through time,

hereinafter referred to as Variable Harmonic Tremor (VHT) (Figure 2-2). These tremors

are comparable to the iceberg-related signals observed by Talandier et al. [2002] at

lower-frequencies (< 32 Hz) using PSN seismic stations. Our sound-channel based

observations indicate a fundamental frequency that is typically within the 4-10 Hz range

(Figure 2-2a,b panel v), but can reach as high of 30 Hz in some instances (Figure 2-2c, panel

v). As many as eight spectral bands can be seen in some tremor packets, with significant power above 80 Hz (Figure 2-2b). VHT signal packets can persist from ~1-30 min, but their occurrence is spatially clustered with periods of activity lasting from hours-to-days.

As illustrated in Figure 2-2 (panels i and ii), VHT signals are commonly exhibit abrupt onsets and terminations, and in some instances these polychromatic signals evolve from or into a continuous monotonic signal (Figure 2-2b) or broadband noise (Figure 2-2abc).

Within a signal packet, azimuthal estimates do not change significantly through time, despite changes in the spectral character of the signal (Figure 2-2abc, panel iii). This suggests that these various portions of the signal packet likely originate from the same source region or within a narrow source zone.

The received signal strengths of the VHTs at DGS range from 119-133 dB re 1μPa and those at CL range from 126-142 dB re 1μPa (peak-to-peak). VHT signals, as identified by the analyst, were seen throughout the year with no clear temporal trend. Many of the loudest and longest duration signals, however, were observed during the Austral fall and winter.

4.2. Localization of VHT Sources

In keeping with the observations of Talandier et al. [2002], a subset of the loudest VHT episodes can be correlated spatially and temporally with a large (~8 x 27 km) iceberg that migrated westward along the eastern Antarctic coast during 2002 and early 2003 (Figure 2-3). This iceberg, B-15D, was originally calved from the same ice mass that spawned the B-15B iceberg tracked by Talandier et al. [2002] within the Ross Sea. The azimuths for six pairs of VHT signals that were recorded at both the CL and DGS stations

are shown in Figure 2-3a, with shaded areas representing error bounds for each signal. Satellite-derived iceberg locations, color coded in time, show the westward migrating iceberg B-15D [National Ice Center (NIC), 2003]. As iceberg positions are not updated daily, we have used iceberg locations on or within three days of the VHT arrivals. For each episode, B-15D locations fall within the error bounds of our azimuthal locations.

The set of possible locations that satisfy the differential arrival time data (ΔT) for stations CL and DGS are shown in Figure 2-3b. These curves also show reasonable agreement with the B-15D locations that are temporally closest to the time of the VHT observations [National Ice Center, 2003]. Assuming a constant velocity medium of 1.475 km/s provided the best agreement between the locations derived from the intersection of the azimuthal pairs (Figure 2-3a) and the differential arrival time locations. Predicted ΔT values for the locations derived from the intersection of azimuthal pairs yield residuals between -13 and 29 seconds (Table 2-1).

Most of the VHT azimuths, however, do not align with drifting icebergs, as tracked by the NIC. Figure 2-4 shows azimuthal paths and locations calculated for all the VHT signals from 2002 through mid-2003, with green and red lines representing azimuths calculated from CL and DGS, respectively. The prevalence of these signals suggests that VHT noises may be generated by smaller icebergs, which are not tracked, but litter the Antarctic shelf region, or that VHT signals also can be generated by coastal ice sources. The Wilkesland region, for example, is populated by a number of outlet glaciers and ice streams, which are distributed throughout the region where azimuthal data indicate the VHT signals are sourced (Figure 2-4). As the ice scrapes over the bedrock and inters the ocean along its grounding line, harmonic signals could be generated in a

manner analogous to an iceberg scraping the shelf. Consistent with this idea, Talandier et al. [2002] have identified at least two tremor episodes not associated with drifting icebergs in January 2001 and November 2000 that appears to source from the Mertz Glacier (~68°S, 145° E) and the Tucker Glacier (~72°S, 170° E), respectively. Our data shows the area near the Mertz glacier to be very active in 2002 and 2003 with several VHT azimuths aligning with this section of the coast. A direct hydroacoustic path does not exist, however, between the hydrophone stations and the Tucker glacier within the Ross Sea region.

5.0. Cusped-Pulsed Tremor (CPT) Observations

5.1. CPT Signal Characterization

A second signal, a cusped-pulsed tremor (CPT) signal, is characterized by curved harmonic bands of energy in the 4-80 Hz frequency range with fundamental frequencies ranging from 4-10 Hz (Figure 2-5). The CPT signals were only seen on 31 days in 2002 and on 7 days in 2003 (as of May 2003), occurring primarily in the Austral fall and winter. The received levels of these signals range from 126-139 dB re 1 μPa at CL and 120-131 dB re 1 μPa at DGS. Their appearance is very similar to some hydroacoustically-observed volcanic tremor [e.g., Dziak and Fox, 2002], with the duration of a single pulse ranging from 25-60 sec and the interval between pulses ranging from 30-90 sec. Pulsed signal trains can last anywhere from 10 min to over 1 hr. They commonly exhibit a near regular pulse spacing (Figure 2-5a); however, some series have pulses at variable intervals (Figure 2-5b).

Azimuth calculations show fixed azimuths throughout each pulse, as well as the entire pulse series (Figure 2-5, panel iii), with pulses exhibiting high correlations

27

coefficients. Unlike the more continuous VHT signals, there is no coherent energy between the pulses (Figure 2-5, panel iv).

5.2. Localization of CPT Sources

CPT azimuthal locations were checked against iceberg locations from the NIC. While icebergs were present within the error bounds of a small minority of signals, the majority of the signals did not originate from known iceberg locations. Moreover, those CPT signals that did have icebergs near their azimuthal track were observed later in the year originating from the same location after the iceberg had drifted out of the error bounds—suggesting that the sources for the CPT signals remain fixed.

Unlike the VHT azimuths that included most of the Antarctic coast from 90°E to 160°E, CPT signals only originate from five geographic areas. CPT azimuths are shown in Figure 2-6a with green and red lines representing azimuths calculated from both CL and DGS, respectively. RADARSAT imagery from the source regions, as estimated from intersecting azimuthal pairs, show small ice streams in each of these areas. Free floating ice blocks are observed trailing off some of the streams, perhaps indicative of ongoing activity.

Figure 2-6b shows sets of possible CPT source locations based on the arrival time differences between the CL and DGS stations. Each curve falls within the errors of our azimuthally calculated source locations, with the absolute values of the T residuals ranging from 0.6-47 sec.

6.0. Discussion

6.1. Sources and Mechanisms

Both signal types are similar to some subareal [e.g., Hagerty et al., 1999; Johnson and Lees, 2000] and submarine [e.g., Dziak and Fox, 2002] volcanic tremor. Location estimates, however, are inconsistent with sources within the volcanically active regions of the Kerguelen Plateau or Ross Sea (Figures 2-4, 2-5 and 2-7). Likewise, azimuthal pair locations (Figures 2-5a and 2-7a) constrain the sources to be too far to the south to be associated with the Southeastern Indian Ridge (SEIR). The pervasiveness of these signals also would imply a much greater eruption frequency than commonly observed along an intermediate-spreading rate ridge systems, and the CPT and VHT signals are not associated with seismic slip events (T-waves), which typically accompany seafloor eruptive activity [e.g., Fox and Dziak, 1998]. It is also noteworthy that most of the SEIR lies below 2000 m water depth; whereas, submarine tremor has thus far been observed only in association with relatively shallow volcanic edifices (depth <1000 mbsl). In these settings, lower pressures may promote tremor generation and the signals should be more efficiently coupled into the sound channel [Talandier and Okal, 1987]. There is no evidence for a longitudinally extensive chain of shallow seamounts extending along the Wilkesland shelf region.

The spatial and temporal correlations outline above (Sections 2-4 and 2-5) argue that the observed tremors are generated in association with drifting icebergs and coastal ice sources, such as outlet glaciers and ice streams. Similarities between the VHT signals described here and ice-related signals reported by Talandier et al. [2002] argue strongly for a common source mechanism. Talandier et al. [2002] have suggested that the harmonic nature of the Ross Sea tremors results from resonance of a drifting iceberg or fluid filled cavity within the iceberg. Seafloor scours from drifting icebergs appear to be

29

common within many polar shelf regions [e.g., Polyak et al., 2001], arguing that this resonance could be excited as the iceberg scrapes the seafloor.

The dominant 4-10 Hz fundamental observed within the VHT signals is consistent with the observations of Talandier et al. [2002]; however, in some instances, these hydroacoustic data show fundamental frequencies exceeding 30 Hz (Figure 2-2c). If similar high-frequency energy was generated during the Ross Sea tremor events, those signals would have been aliased by the PSN seismic sensors—as would many of the high-order overtones in Figure 2-2. Talandier et al. [2002] and Okal et al. [2002] have discussed possible types of resonators in some detail. As they point out, the lowest frequency ~3 Hz fundamentals would corresponded to the eigenfrequency of a vertical shear mode within a ~300 m thick ice layer (assuming β=1.8 km/s). This thickness is consistent with that predicted for iceberg B-15, and sufficient to allow the ice mass to scrape across portions of the shelf. Higher-frequency fundamentals (~10-30 Hz) would suggest resonance within an ice layer having a thickness of only a few tens of meters. The observation shown in of Figure 2-2c indicate the pitch of the resonator can evolve from 30 to 8 Hz during a period of a few minutes, suggestion that different portions of variable thickness ice mass are resonating or that the physical properties of the resonator are evolving rapidly.

Other possible resonator scenarios include the excitation of a fluid (water and air) filled cavities within the ice, making the eigenfrequency a complex function of the cavity's shape and size, as well as the impedance contrast between the fluid and surrounding ice mass [Chouet et al., 1988; Garces and McNutt, 1997]. Changes in these

parameters during ice movement could help to explain spectral fluctuations during the tremor events [Talandier et al., 2002].

Despite the correlation of some VHT signals with a large iceberg being tracked by the NIC, our observations suggest that tremor signals also may be linked to the movement of smaller icebergs and/or coastal ice sources along eastern Antarctica. As shown in Figure 2-7, there is a rough correlation between VHT signal azimuth and the predicted azimuths to named outlet glaciers along the portions of the coast with unblocks propagation paths to the CL hydrophone. The land-based portion of these glacial ice masses and their glacial tongues are known to be active in many areas. These ice tongues extend over the water where they can break up into smaller blocks of ice that could become mobile due to the influence of wind and waves [Menzies et al., 1995]. As with drifting icebergs, acoustic signals generated within or near these tongues could radiate energy into the water column.

The abrupt onset and termination of many of the VHT and CPT signals (Figures 2-2 and 2-5) suggests the ice is moving in stick-slip manner, and there is mounting evidence for such behavior within Antarctic glaciers and ice streams. For example, a continuous GPS study recently demonstrated tidally influenced stick-slip motion within a Siple Coast ice stream in western Antarctica. Individual slip events lasted from 10 to 30 minutes with an average slip velocity of ~1 m/hr [Bindschadler, 2003]. This duration is similar to the VHT signals observed in the IMS hydroacoustic data, and the surging nature of the ice movement could act to excite these tremor signals. Similarly, Ekstrom et al. [2003] have identified a series of unusual long-period surface wave events (equivalent to a > 4.5 M earthquake) located in glacial regions, including tectonically stable areas such as

31

Greenland and coastal Antarctica. The radiation pattern of these events can be described by a single force couple model (applicable for landslide events), as opposed to a standard double-couple earthquake source. This led the authors to suggest that these events were generated by stick-slip glacial quakes. Two of these glacial quakes were located within the Wilkesland region, albeit hundreds of kilometers inland ($\sim$67° S, 110° E) from the coastal regions that source the tremor signals.

The instantaneous velocities and style of movement of the coastal Wilkesland glaciers and ice streams are not presently constrained. Long-term slip rates derived from Landsat imagery of the Mertz Glacier ($\sim$68°S, 145° E), however, show velocities almost twice as large as many of the ice streams along the Siple Coast, exceeding 1000 m/year [Scambos et al., 2000a]. If this displacement is taken up during periods of stick-slip motion with instantaneous velocities similar to the 1 m/hr observed by Bindschadler et al. [2003], then more than 1000 hrs of slip could be expected annually within the Mertz Glacier alone.

Although CPT signals are observed to originate from a subset of the active ice streams within the Wilkesland region, the environmental conditions necessary to generate these signals are not well constrained. The near uniform spacing of CPT signals is reminiscent of a geyser-like process, as observed within subareal volcanic systems. Consequently, we speculate that the process may be hydrologically driven, with a periodic recharge that allows the glacier to slip in a repeating manner. Thus far, CPT signals have only been observed in the Austral fall and winter months. This seasonality must be verified over a longer period of observation; however, such temporal behavior could reflect a change in the hydrologic regime and the development of a uniform

subglacial hydrous layer that allows the ice streams to move in a more continuous manner during the warmer months [Menzies, 1995]. It is not clear why some ice streams generate CPT signals and others do not.

6.2. Propagation of Sound from the High Southern Latitudes

In high latitude regions, colder oceanic temperature profiles do not facilitate the existence of a deep sound channel. Acoustic energy from a shallow depth source along the Wilkesland shelf must initially propagate as a surface reflected phase, crossing the Antarctic convergence zone, and later becoming coupled within the mid-latitude sound channel. In Figure 2-8, a parabolic equation (PE) code [Smith, 2001] is used to investigate propagation from a source near the Mertz Glacier to the SOFAR moored hydrophone triad CL. This model confirms that energy can be transferred through the Antarctic convergence zone and into the deep sound channel (Figure 2-8). Transmission loss estimates implying maximum source levels of ~245 dB re 1µPa @ 1 m. This is equivalent to a small airgun array [cf., Richardson et al., 1998]. However, unlike the short duration transient signals generated by an airgun array, the tremor signals represent a long-duration noise source that is more continuous in its nature.

7.0. Conclusions

During the period January 2002 through May 2003, two distinct types of hydroacoustic tremor were recorded on IMS hydrophone stations within the Indian Ocean—variable harmonic tremors (VHTs), which are characterized by continuous harmonic bands with spectral peaks that fluctuate in frequency through time, and cusped pulse tremors (CPTs), which are short pulses having a convex-upward appearance in a spectrogram. The harmonic nature of these signals supports the idea of resonating ice

masses, as proposed by Talandier et al. [2002]. Azimuthal calculations allow us to locate specific areas of active ice movement, and in combination with satellite-based observations, suggest that both signals are sourced from the near coastal regions of Wilkesland, eastern Antarctica. A subset of the loudest VHT signals can be correlated temporally and spatially with the westward migration of a large iceberg across the shelf region. The prevalence of VHT signals, however, suggests that they may also be generated in association with the many smaller, unnamed icebergs as well as ice streams and their tongue extensions.

Ice-generated tremor signals can be detected at near-equatorial latitudes, over 6000 km away. Sound propagates first as a sea surface reflected phase at high southern latitudes, with energy transferred in the deep sound channel that develops to the north of the Antarctic convergence zone. The peak-to-peak source level of the observed tremors may be as large as ~245 dB re 1 μPa @ m. This is equivalent to the source level of a small active source airgun array. However, relative to airgun transients with sub-second pulse duration, tremors may persist continuously for up to 30 minutes—dominating the noise spectra during some time periods. Conceivably, warming in the Antarctic region [e.g., King and Comiso, 2003] and the degradation of the Antarctic ice sheets [e.g., Scambos et al., 2000b] has increased the amount of free-floating ice and modified the dynamics of outlet glaciers and ice streams. Due to the absence of historical data, however, it is not known if the noise contribution from these types of ice-generated signals has increased in recent years.

.

Tables

Table 2-1. Correlation of VHT signals with B-15D.

Hydrophone arrival Date	NSIDC date	Arrival at CL	Arrival at DGS	NSIDC location	Azimuthal location*	Residual ΔT (seconds)
2002, 113	2002, 115	12:43:30	13:33:30	65.4°S, 143.4°E	64.9°S, 139.0°E	8.889
2002, 289	2002, 289	06:45:43	07:32:05	65.4°S, 123.5°E	65.7°S, 122.8°E	25.032
2003, 087	2003, 089	03:41:13	04:24:12	65.1°S, 115.5°E	65.9°S, 114.9°E	27.096
2003, 099	2003, 103	16:00:01	16:42:24	65.3°S, 109.6°E	65.1°S, 110.8°E	-1.081
2003, 128	2003, 131	23:32:55	00:10:50**	65.0°S, 101.9°E	64.8°S, 101.4°E	29.221
2003, 158	2003, 159	20:00:58	30:34:26	63.7°S, 096.9°E	63.9°S, 094.3°E	-13.096

* Locations derived by interpolating latitude and longitude positions at azimuth intersections
** Arrival at DGS on the following day 2003, 129

Figure Captions

Figure 2-1. Map of Indian Ocean Basin study area. Blue stars indicate hydrophone triad locations labeled as CL (Cape Leeuwin), DGS (Diego Garcia South) and DGN (Diego Garcia North. Mid-ocean ridges shown as black lines with the following geographic location labels: Southeast Indian Ridge (SEIR), Australian-Antarctic Discordance (AAD), Ninety East Ridge, Kerguelen Plateau, Wilkesland section of Antarctica. Color bar indicates sea floor bathymetry in meters relative to sea level.

Figure 2-2. (a, b, c) Signal (i), spectrogram (ii), azimuth (iii), correlation coefficient of azimuthal calculation (iv), and power spectral density plots (v) of three different VHT signals recorded on CL hydrophones in 2002, Julian Day (JD) 113 at 12:36; 2003, JD 128 at 23:31; and 2002, JD 208 04:19, respectively. Note the harmonic bands of energy with fundamental frequency at ~7, ~9, and ~8 Hz respectively and the variation in spectral content as each signal progresses with time. Red dots on the azimuth and correlation coefficient panels represent points where the slowness velocity was 1.485 ± 0.03 km/sec. The abrupt onset and termination of these signals are typical of VHTs. Azimuth calculations were done on a bandpass filtered (5 to 35 Hz) signal using 5 second windows with 50% overlap. During periods with little broadband energy, the cross correlations exhibit significant structure, leading to unstable azimuth estimates. Power spectral density calculations were done on the boxed portion of the spectrogram (45 sec), using a zero padding and Hanning window.

35

Figure 2-3. a.) Azimuths of six VHT signals from CL and DGS hydrophones along with iceberg locations. Each colored circle represents the National Ice Center (NIC) location of iceberg B-15D at various times throughout 2002 and 2003 (steady westerly migration). Each colored path corresponds to the azimuth and error bounds (±1.26 degrees for CL and ±1.51 for DGS derived from known earthquake locations) calculated from signals arriving at CL and DGS hydrophones within three days of the NIC reported locations. Black stars represent hydrophone locations. b.) Differential travel time curves for each of the six VHT signals. Each curve represents a set of locations yielding the calculated arrival time differences using a 3 x 3 km spaced grid and a sound velocity of 1.475 km/sec. Red dots indicate our iceberg locations derived from azimuths, and dark blue dots indicate NIC locations.

Figure 2-4. Azimuthal traces for VHT signals recorded on CL hydrophones (green) and DGS hydrophones (red) in 2002 and 2003. Blue dots indicate USGS named glaciers, red dots indicate locations for glacial tongues, and black stars represent hydrophone locations. Note the gaps between azimuth paths where no glaciers and ice streams are present. The deficiency in azimuths falling west of 90°E is a result of partial blockage from the geography of the Antarctic coast and the Kerguelen Plateau, and an absence of azimuths east of 160°E may reflect the limits of our detection capabilities. There are a small number of easterly CL azimuths (<150 degrees) relative to the total number of azimuths that appear to originate from higher latitudes for which we have no explanation.

Figure 2-5. (a and b). Signal (i), spectrogram (ii), azimuth (iii), correlation coefficients of azimuth (iv), and power spectral density plot (v) of pulses in a regularly spaces CPT series (a.) and in an irregularly spaced CPT series (b.) recorded on CL hydrophones starting at 2002, JD 160 at 11:07 and 2002, JD 177 at 20:43 respectively. The fundamental frequencies of the series are ~9 and ~6 Hz with harmonics up to at least 35 Hz. Red dots on the azimuth and correlation coefficient panels represent points where

the slowness velocity was 1.485 ± 0.03 km/sec. Azimuth calculations were done on a bandpass filtered (5 to 35 Hz) signal using 5 second windows with 50% overlap, and power spectral density plots were done on the boxed portion of the spectrogram (20 sec) using a zero padding and Hanning window

Figure 2-6. a.) Azimuthal traces for CPT signals recorded on CL hydrophones (green) and DGS hydrophones (red) in 2002 and 2003. Blue dots indicate USGS names glaciers, red dots represent glacier tongue locations, and black stars represent hydrophone locations. The red squares show areas where RADARSAT images are taken and the figures around the map are the corresponding satellite images. Blue dots on the images are the same glacier locations as those on the map. Note the presence of several different ice streams connecting the glaciers to the ocean. Some ice streams also have floating blocks of ice trailing from the ends of the streams, which may be indicative of on-going activity. b.) Differential travel time curves for the CPT series where DGS data produced reasonable azimuths. Each curve represents a set of locations yielding the calculated arrival time differences using a 3 km by 3 km spaced grid and a sound velocity of 1.475 km/sec. Red dots indicate the CPT locations for each travel time curve. Note some curves overlap for different CPT locations.

Figure 2-7. Histogram of VHT azimuths (blue), glaciers azimuths (green) and glacier tongue azimuths (red) calculated using one degree bins for the CL data only. The azimuths for the glaciers and glacier tongues were calculated from station CL to each USGS location. The dashed black lines confine the area where we have the most confidence in our azimuths with the higher azimuth cut-off due to bathymetric blockage and the lower azimuth cutoff due to anomalous source locations. The black lines to either side of the highest VHT peak represent our errors in azimuthal calculations. Note the similar trend in number of glaciers with number of VHT signals.

Figure 2-8. a) Transmission loss model for a 40-Hz source at a depth of 100 m near the Mertz Glacier (~86 S, 145 E). The Cape Leeuwin receiver is located at a depth of 1100 m at a range of ~4100 m. Range dependant sediment thickness is derived from a NOAA

sediment thickness database and range dependant sound velocity profiles are taken from the US Navy's Generalized Digital Environmental Model (GDEM) for the month of July (30 minute resolution). Sediment properties: 1600 m/s sound speed, density 1500 kg/m^3 and compressional attenuation of 0.15 dB/m/kHz. Deep bottom properties: 2300 m/s sound speed, density 2210 kg/m^3 and compressional attenuation of 0.05 dB/m/kHz. The parabolic equation code UMPE2DBB was used in this calculation [Smith, 2001]. Transmission loss between the source and reciever is estimated to be ~103 dB re 1 uPa. b) Sample sound velocity profiles along the propagation path.

Figure 2-1

Figure 2-2

40

a.

b.

2002, JD 113 ●
2002, JD 289 ●
2003, JD 087 ●
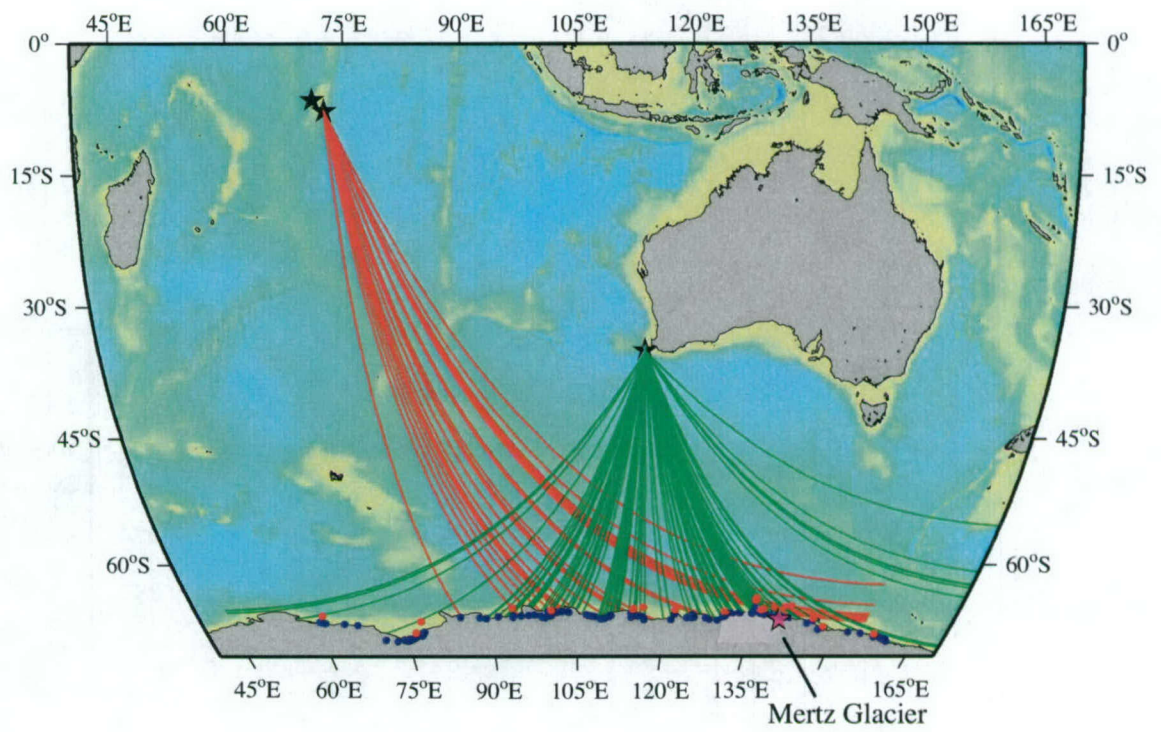2003, JD 099 ●
2003, JD 128 ●
2003, JD 152 ●

Figure 2-3

41

Mertz Glacier
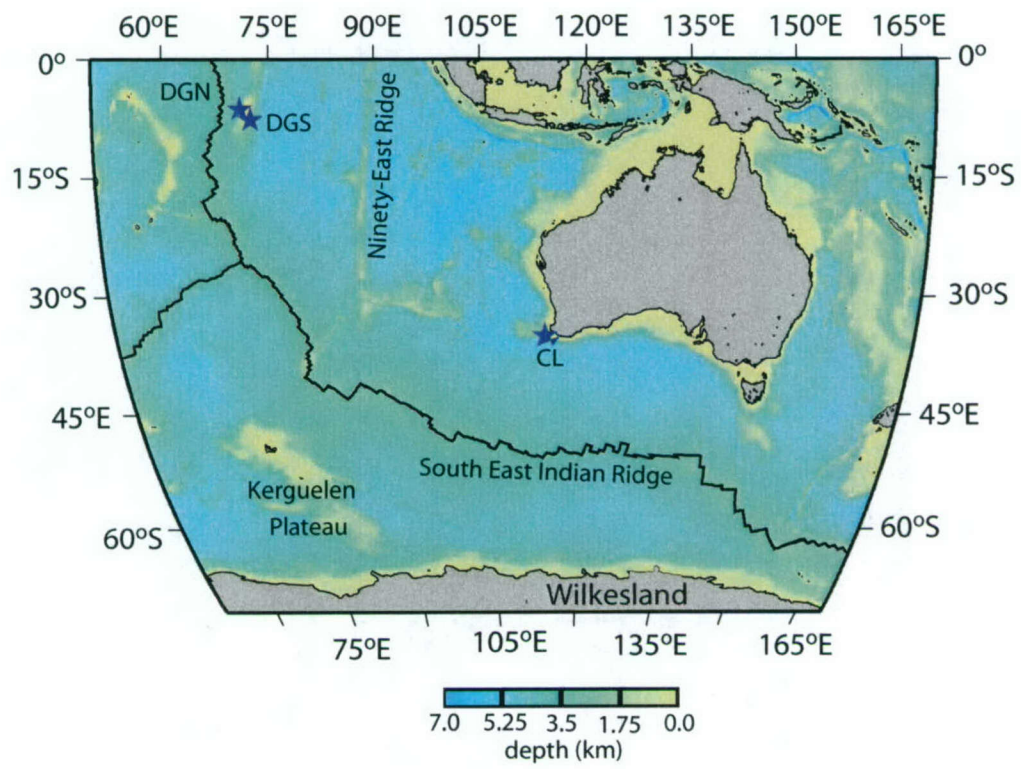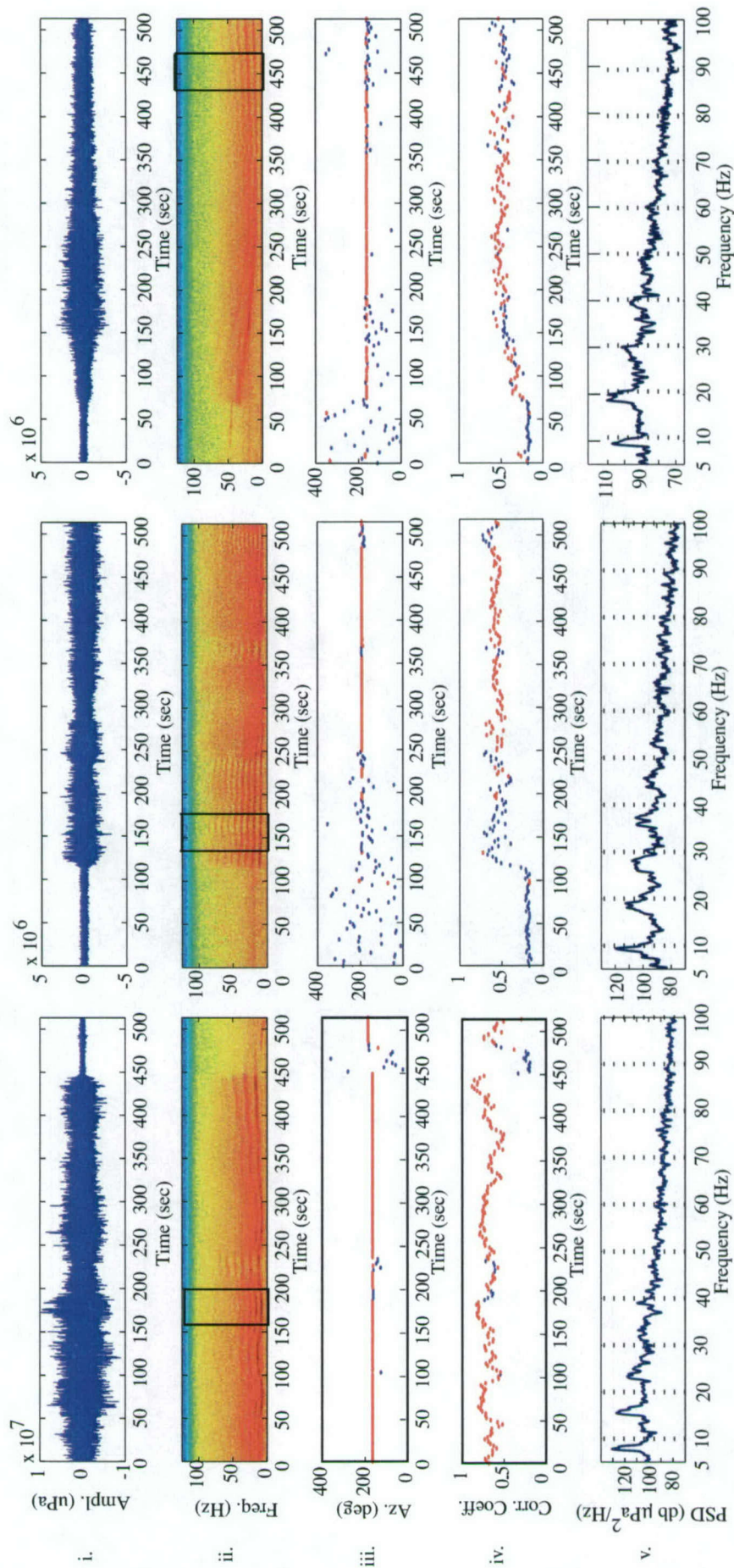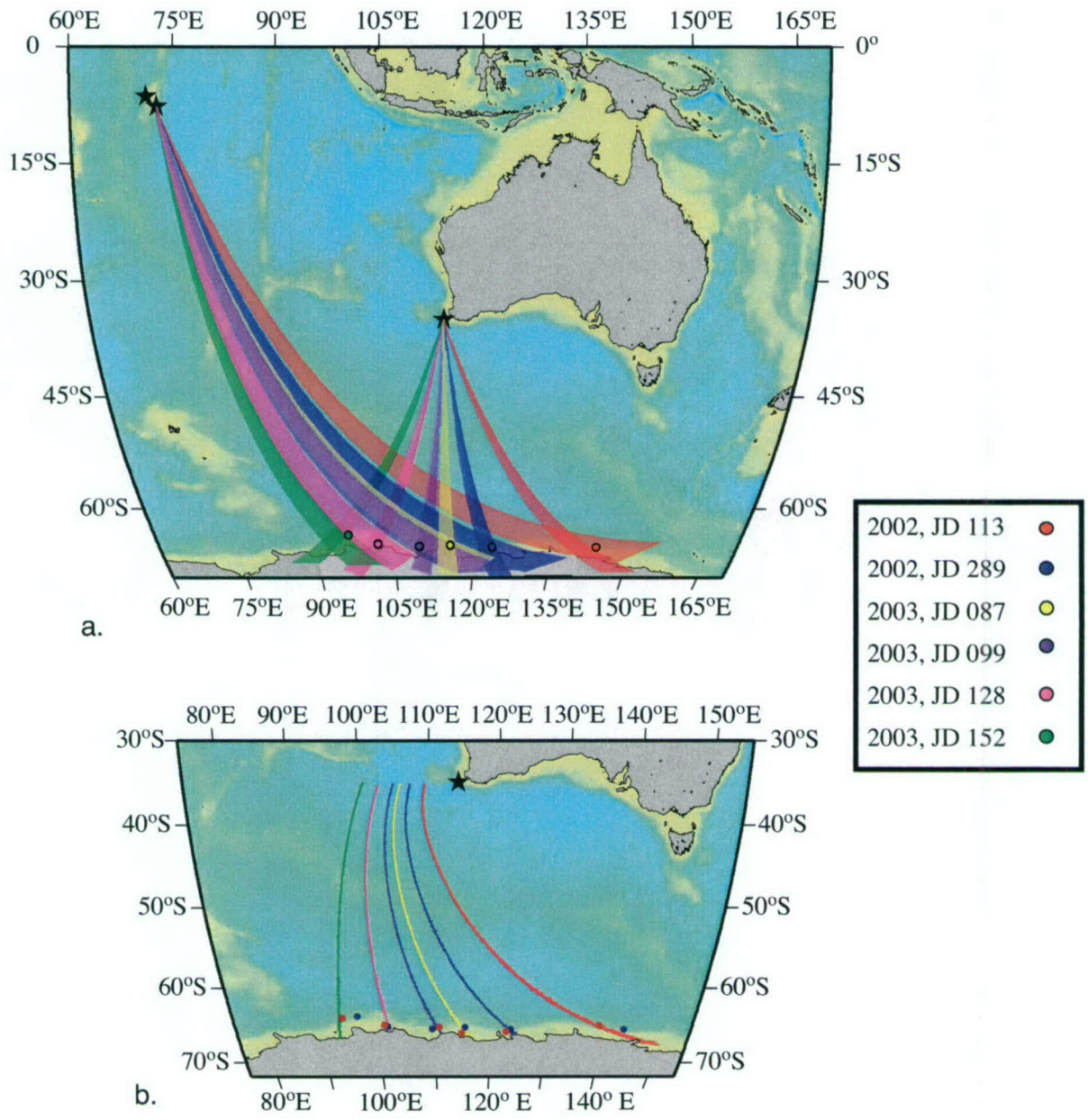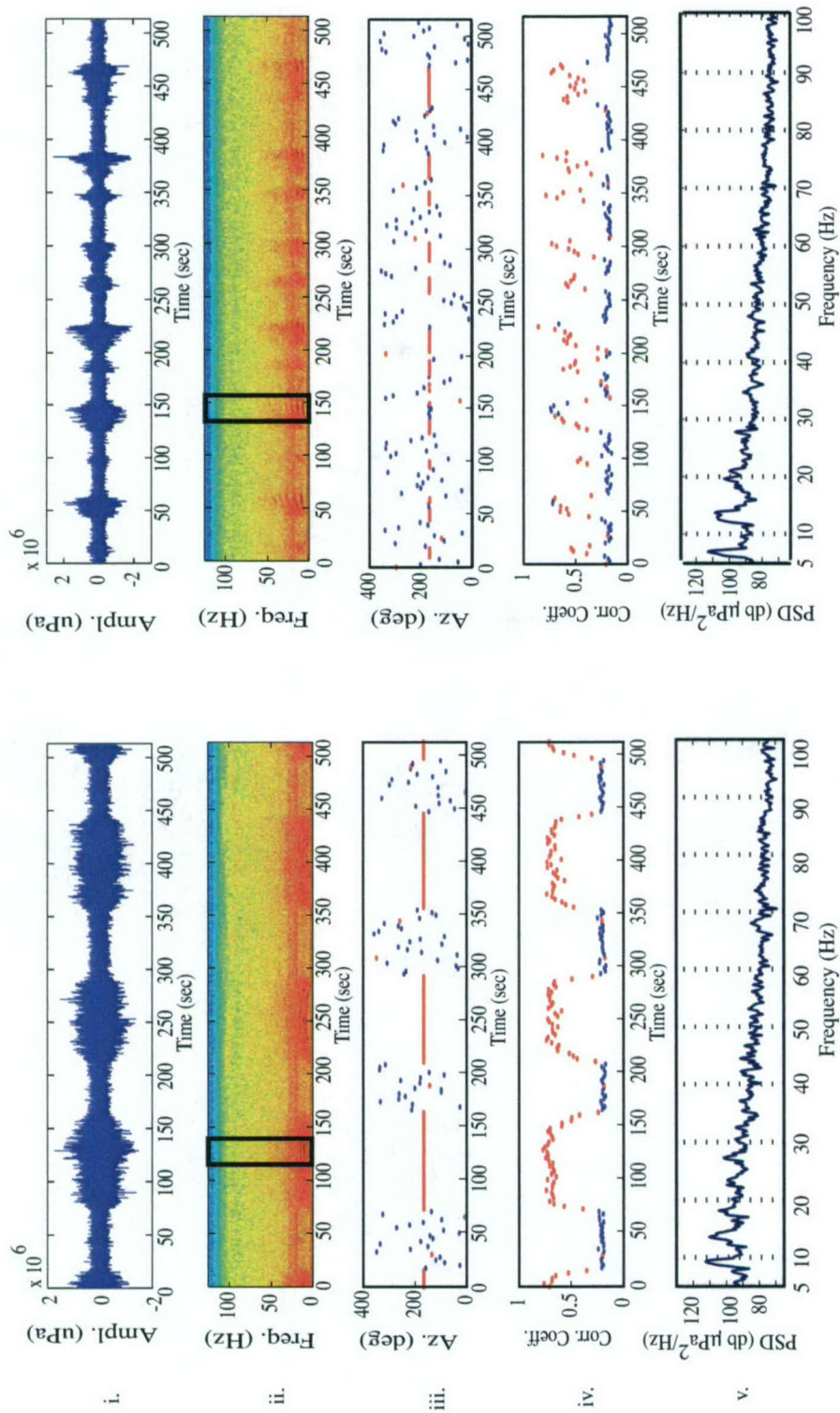
Figure 2-4

Figure 2-5

Figure 2-6

Figure 2-7

Transmission Loss (dB re 1m)

a)

b)

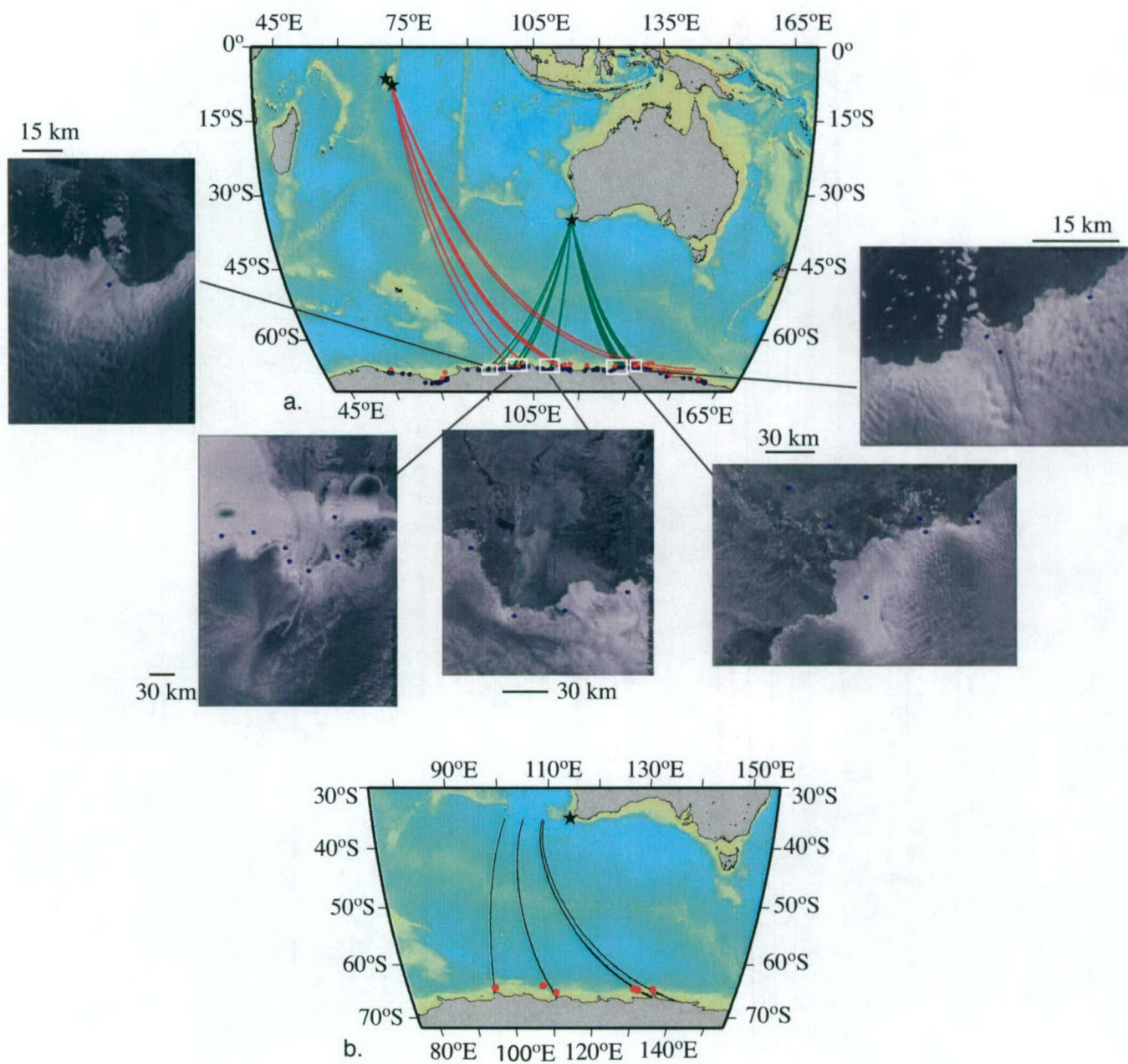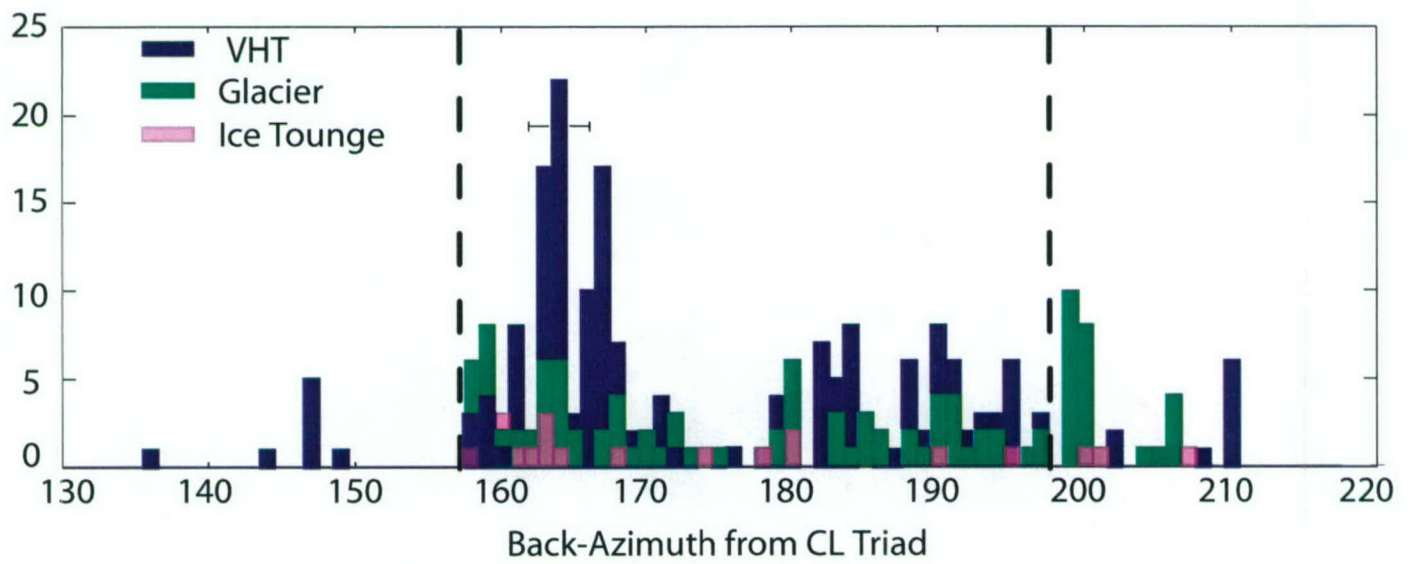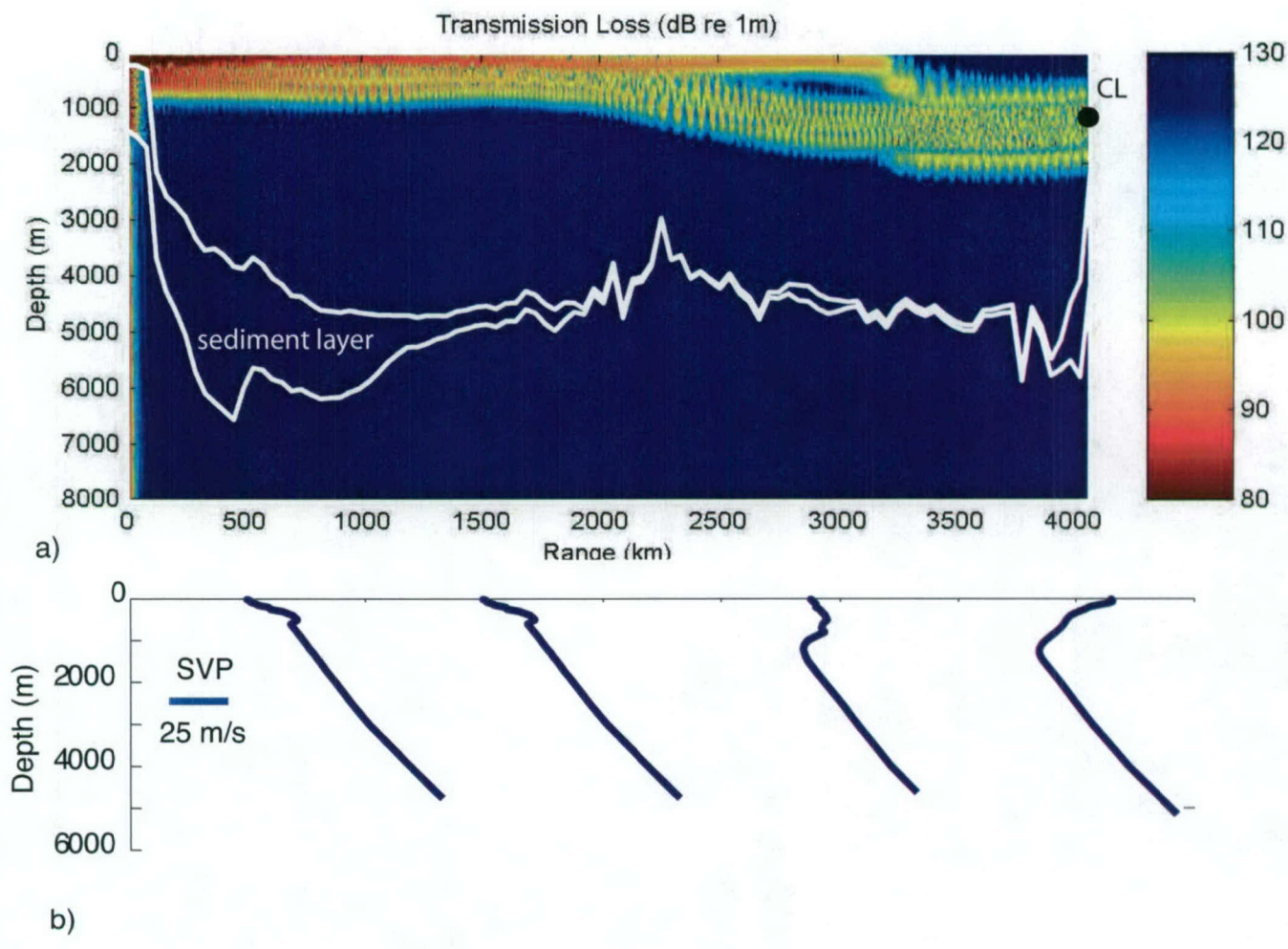**Figure 2-8**

Blockage of High Frequency energy from Earthquake Sources

On July 15, 2003, an extremely large (7.6 Mw) earthquake occurred in the northwest Indian Ocean [Bohnenstiehl *et al.*, 2004]. Comparison of arrivals at Diego Garcia North, Diego Garcia South and Cape Leeuwin stations shows a strong T-wave arrival at Diego Garcia North, a barely visible lower-frequency T-wave arrival at Diego Garcia South and a strong high-frequency arrival at Cape Leeuwin (Figure 3-1), despite apparent blockage along the direct path from much of the rupture plane to this station. This large event, along with its well-located aftershocks, allows some interesting observations to be made regarding blockage.
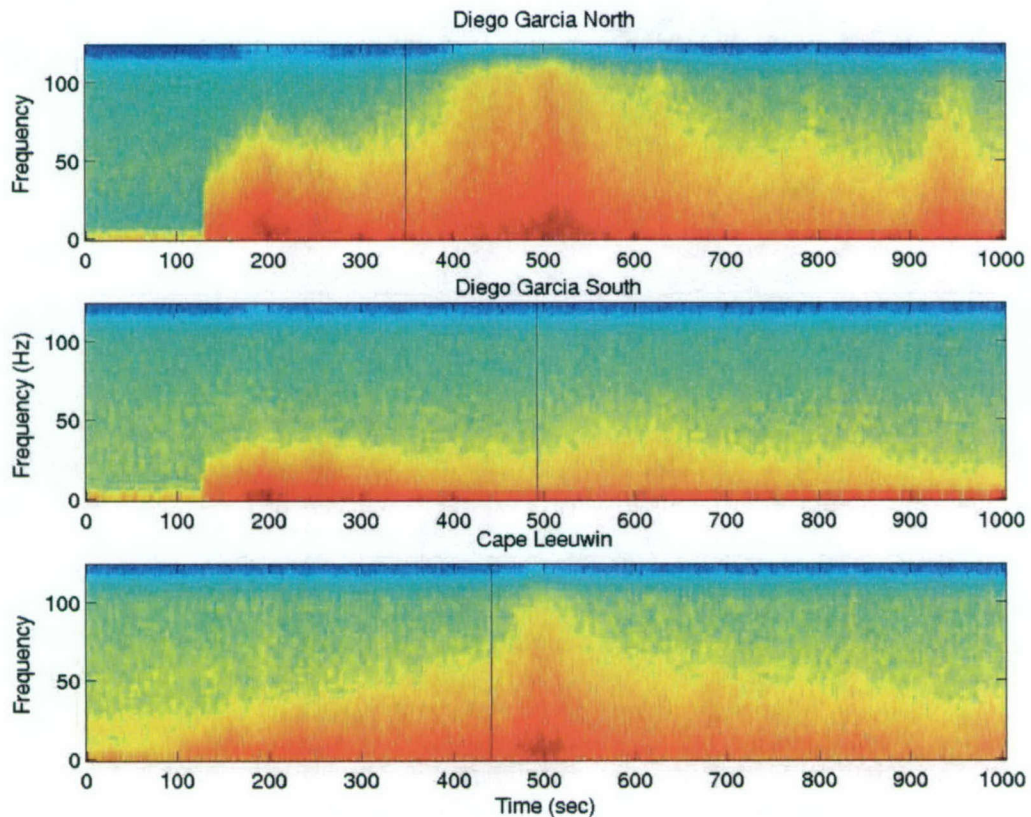

Figure 3-1. Spectrogram for earthquake arrival at Diego Garcia North (top), Diego Garcia South (middle), and Cape Leeuwin (bottom). Thin vertical black line indicates predicted start time of T-wave arrival. Abrupt P-wave arrivals are evident at both Diego Garcia stations. Cape Leeuwin shows a prolonged build up of energy before the primary T-wave.
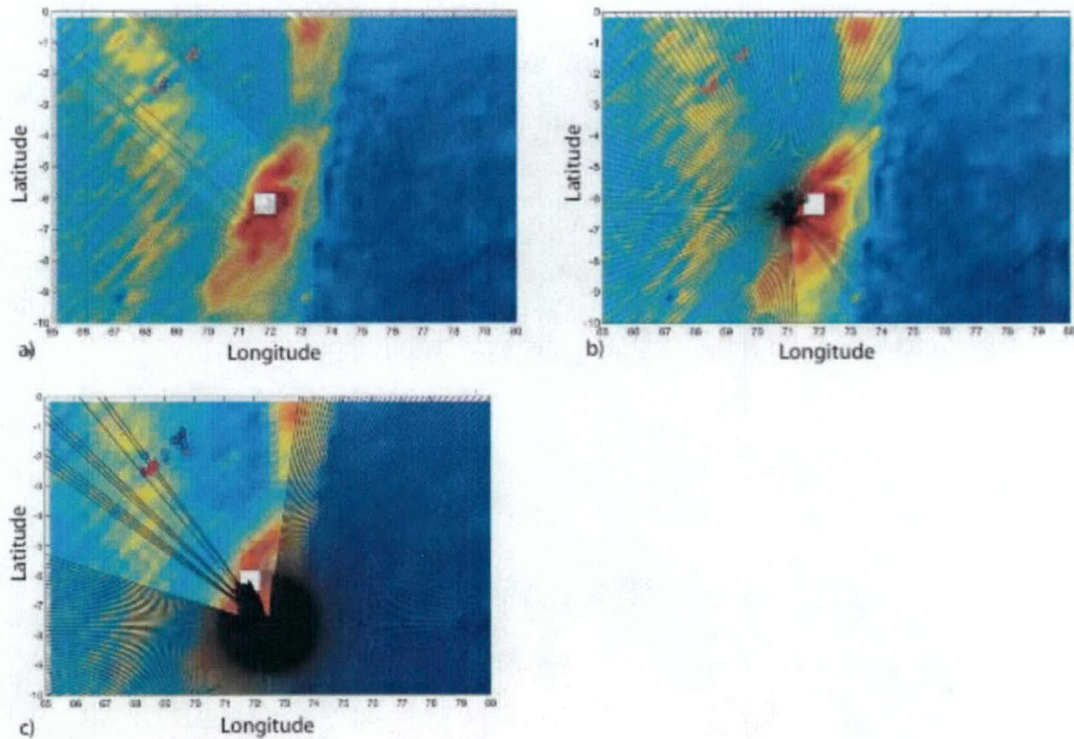
Figure 3-2. Blockage maps with 50 m stop criteria and 1 degree rays for Cape Leeuwin (a), Diego Garcia North (b) and Diego Garcia South (c). Red circles – detected aftershocks. Blue circles – not detected aftershocks.

Figure 3-2 shows blockage maps for all three stations with a 50-m cut off, and earthquake locations color coded to indicate if they were observed (red) or not (blue) at the given station. The maps show that the 50-m cut off is a fairly good indication of when signals will be blocked. However, those observed signals that traveled over relatively shallow areas were quite weak and lacking in high-frequency energy.

The strike-slip mainshock event ruptured ~210 km of crust, with an estimated rupture duration of ~65 seconds. T-wave azimuths from arrivals at Diego Garcia North indicate that the bulk of the T-wave energy was generated at the moment centroid location, which is consistent with that being the location of the maximum earthquake energy release.

Arrivals at Cape Leeuwin, particularly for the mainshock provide some surprising results. Travel-time and azimuthal analysis suggest that the earliest T-wave arrival at Cape Leeuwin consists of converted P- and S-wave energy from the eastern scarp of the Chagos and Maldives Archipelagos, at distances of several hundred kilometers from the earthquake rupture. Figure 3-3 shows the varying azimuth associated with the long T-wave arrival at Cape Leeuwin, along with predicted arrival azimuths and times for P-wave and S-wave energy from the epicenter, moment centroid and end of rupture for a variety of bathymetric features (Figure 3-4).

The direct T-wave energy, which arrives at a time consistent with an exclusively water-borne pathway, comes in at an azimuth a little to the north of the end of the rupture, and aligned with a deeper area between the Chagos and Maldives Archipelagos. It appears therefore that the energy

was either refraction around the northern area of the Chagos bathymetric highs, or that it represents significant excitation of the seafloor north of the actual rupture zone. The latter is reasonable given the magnitude of the earthquake and the relative roughness of the seafloor adjacent to this slow spreading ridge segment. This arrival is the only portion of the T-wave train that contains significant high-frequency energy. Lower energy reflections from Maldives bathymetric highs to the north and east of the rupture zone are evident within the T-wave coda and show azimuths consistent with the Maldives submerged plateaus.
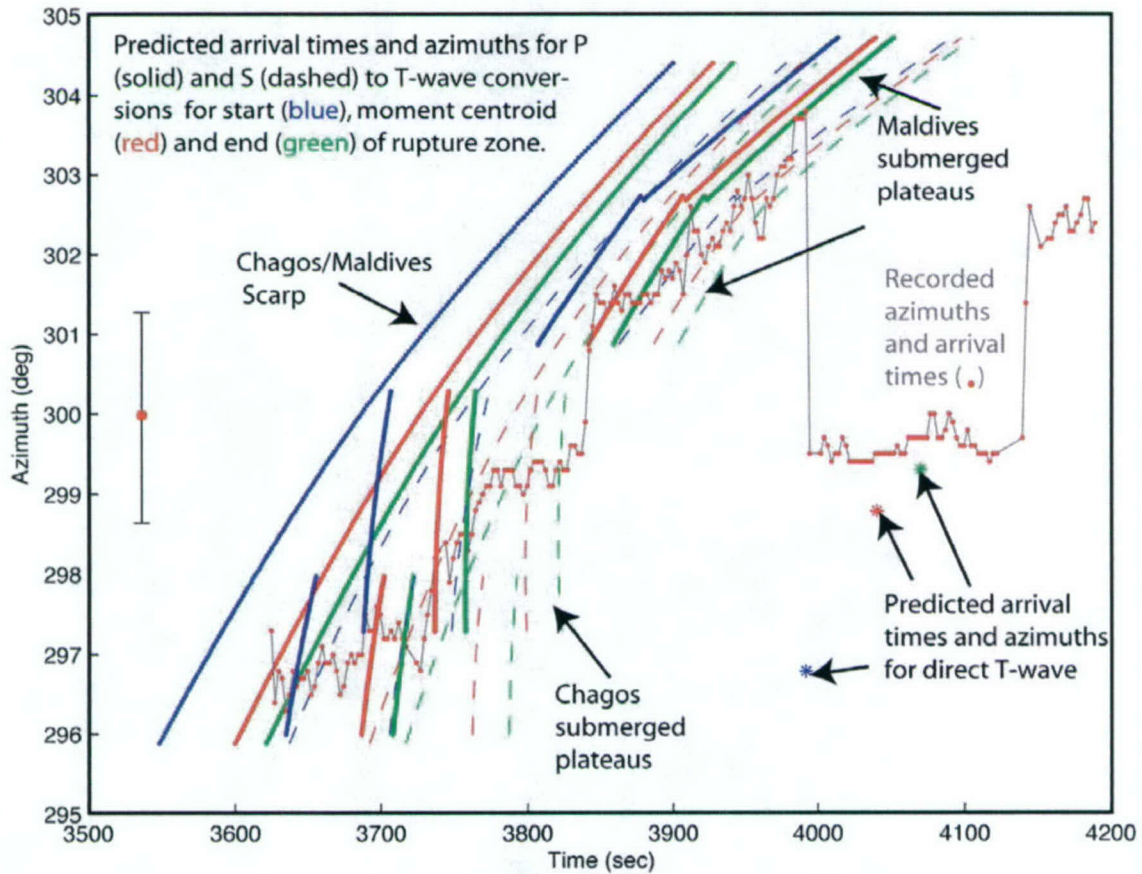

Figure 3-3. Calculated azimuths (red dots) for the T-wave arrival at Cape Leeuwin (see Figure 3-1 – bottom) compared with predicted arrival times and azimuths for P-wave (solid lines) and S-wave (dashed lines) that converted to T-waves on various bathymetric features of the Chagos and Maldives Archipelagos (see Figure 3-4). Predictions are made for energy coming from the start of the rupture (blue), the centroid moment (red) and the end of the rupture (green). Also shown are predicted arrival times and azimuths for the direct T-wave arrival (*). Note last set of azimuths (~4150-4200 seconds) may indicate a reflected arrival from the more northern features on the Maldives Archipelago.
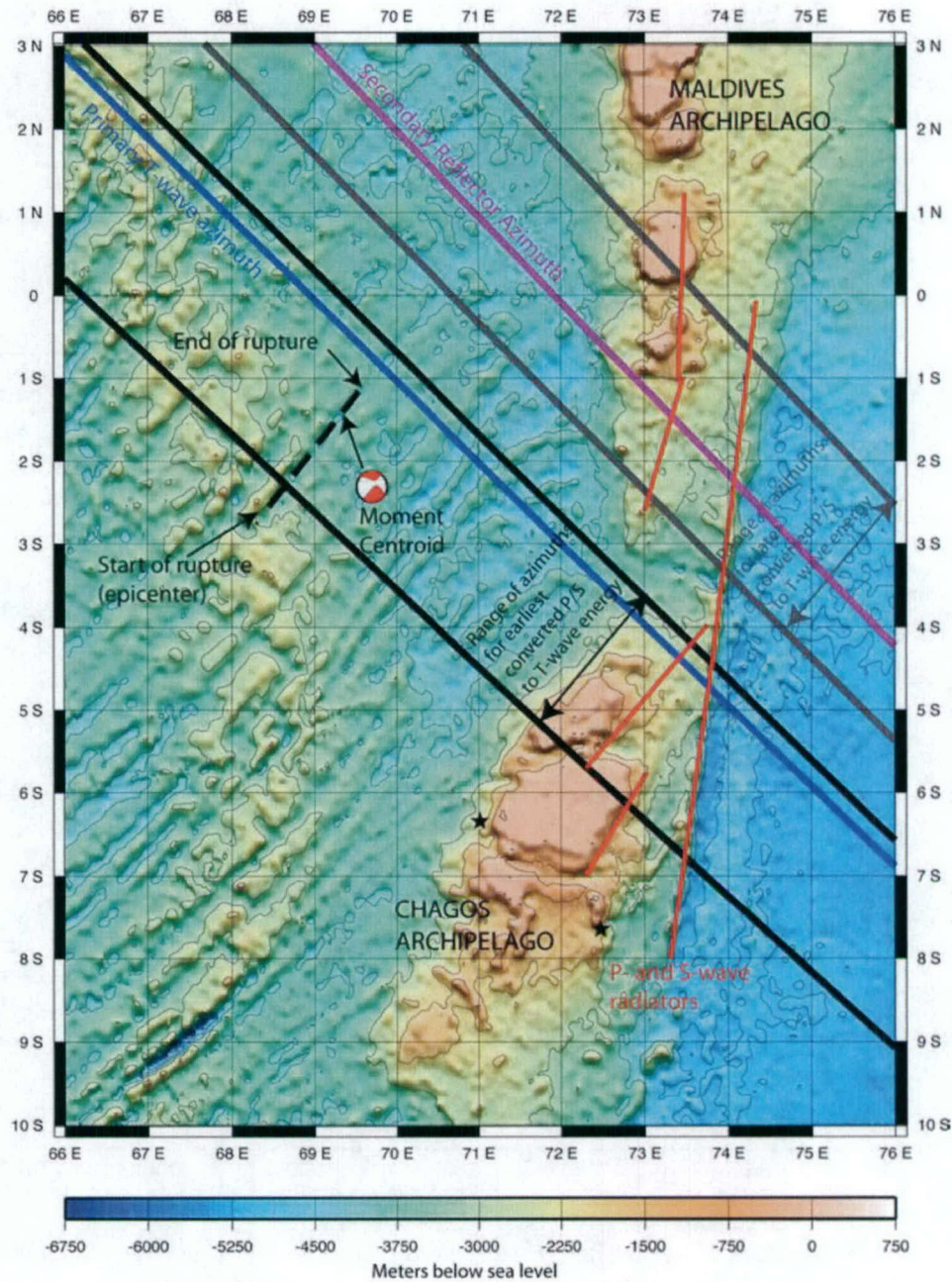
Figure 3-4. Primary bathymetric features associated with Cape Leeuwin T-wave arrival from July 15th, 2003 7.6 Mw earthquake. Earthquake rupture area is indicated by the dashed black line with the start, moment centroid, and end positions noted. Black and gray lines indicate the range of azimuths for converted P/S-wave to T-wave energy observed for the earlier and later arrivals respectively (see Figure 3-3). Red lines indicate likely radiators, with arrival times modeled in Figure 3-3. The blue and purple lines indicate azimuths for the primary high frequency direct T-wave arrival and a later reflected arrival respectively.

Conclusions

We have characterized and quantified hydroacoustic signals in the Indian Ocean Basin for all available data in 2002, as well as characterizing the background noise at each site and confirming that overall Diego Garcia North is the quiestest, and Cape Leeuwin is the noisiest. Beyond weather related influences, specific noise sources include anthropogenic signals such as ship noise, airguns and explosions, as well as geological and biological such as earthquakes and whale calls. The dominant anthropogenic noise is ship noise, which for instance is apparent at Diego Garcia South for > 90% of the time. The dominant natural signals are earthquakes, whale calls and iceberg related signals. At certain times whale calls appear to be so frequent that background noise levels are observed to be raised by several dB in the frequency band specific to that whale call.

We have characterized two hydroacoustic sources capable of exciting high-frequency energy that propagates over 8000 km through the Indian Ocean. From hydroacoustic data, azimuth calculations and satellite imagery, we have defined surging ice streams and drifting icebergs as the dominant signal generators along the coastal sections of Wilkesland, eastern Antarctica. The harmonic nature of these signals supports the idea of resonating ice masses, and the calculated azimuths allow specific areas of active ice movement to be located. These naturally occurring sources provide excellent tools for more details studies of long-range propagation of high-frequency energy through the ACZ.

To better utilize these natural sources, ground-truthing of source locations and near field characterization of the signals should be accomplished through hydrophone measurements made within 10-100's of km of the source, well within the ACZ. Utilizing such tools would allow individual sources to be well located and provide an improved source model for use in investigating propagation across the ACZ.

Our studies of hydroacoustic blockage support the idea that T-wave energy can be generated from multiple scatters. It also appears that high frequency energy generated by near-field scattering from the seafloor may be detected, even though the direct path may be partially or completely blocked. This scattered energy represents the highest frequency, highest amplitude portion of the arrival for the July 15, 2003 mainshock. While blockage appears fairly complete for smaller events when bathymetry of < 50 m is encountered, some energy is still transmitted at relatively shallow depths > 50 m. Further rigorous analysis of large earthquake sources of opportunity would help confirm these observations, and provide more detailed understanding of the processes.

References

Chouet, B. Resonance of a fluid-driven crack: Radiation properties and implications for the source of long-period events and harmonic tremor, J. Geophys. Res., 93, 4375-4400, 1988.

Barkov, N. I., Ice Shelves of Antarctica, *ed*. E. S. Korotkevich, A. A. Balkema, Rotterdam, pp. 26-31, 1985.

Bindschadler R.A., M. A. King, R. B. Alley, S. Anandakrishnan, L. Padman, Tidally controlled stick-slip discharge of a West Antarctic ice stream, *Science*, **301**, 1087, 2003.

Bohnenstiehl, D.R., and M. Tolstoy, Comparison of teleseismically and hydroacoustically derived earthquake locations along the north-central Mid-Atlantic Ridge and Equatorial East Pacific Rise, *Seismol. Res. Lett.,* 74: 790-801, 2003.

Collins, M.D., A split-step Pade, solution for the parabolic equation method, J. Acoust. Soc. Am., Proc 93, pp. 1736-1742, 1993.

Curtis, K.R., B.M. Howe, and J.A. Mercer, Low-frequency ambient sound in the North Pacific: Long time series observations, *J. Acoust. Soc. Am.*, **106**, 3189-3200, 1999.

Del Pezzo, E. and F. Giudicepietro, Plane wave fitting method for a plane, small aperture, short period seismic array: a MATHCAD program, *Comp. Geosc.,* 28, 59-64, 2002.

Dziak, R.P., and C.G. Fox, Evidence of harmonic tremor from a submarione volcano detected across the Pacific Ocean basin, *Jo. Geoph. Res.*, **107**, 10,1029, 2002.

Ekstrom, G., M. Nettles, and G.A. Abers, Glacial earthquakes, Science, **302**, 662-624, 2003.

Eggen, C., and B. D. Dushaw, 2002. A MATLAB Driven GUI Supporting Computation of a Two-Dimensional Field of View and Simulation of Propagation between Points. MTS/IEEE Conference October 29-31, 2002, Biloxi, MS, Abstract number 612.

Fox, C.G., H. Matsumoto, and T.K.A. Lau, Monitoring Pacific Ocean seismicity from an autonomous hydrophone array, J. Geophys. Res., **106**, 4183-4206, 2001.

Fox, C.G. and R.P. Dziak, Hydroacoustic Detection of Volcanic Activity on the Gorda Ridge, February - March 1996, Deep Sea Res. II, **45,** 2513-2530, 1998.

Garces, M.A., S. R. McNutt, Theory of the airborn sound field generated in a resonant magma conduit, *Jo. of Vol. and Geoth. Res.,* **78**, 155, 1997.

Hagerty, M.T. , S.Y. Schwartz, M.A. Garces, M. Protti, Analysis of seismic and acoustic observations at Arenal Volcano, Costa Rica, 1995-1997, J. Vol. and Geoth. Res., **101**, 27-65, 2000.

Hanson, J. A. and H.K. Givens, Accurate azimuthal estimates from large aperture hydrophone array using T-phase waveforms. Geophys. Res. Lett., 25, 365-368, 1998.

King, J.C., and J.C. Comiso, The spatial coherence of interannual temperature trends in the Antarctic Peninsula, Geophys. Res. Lett., 30, doi:10.1029/2002GL015580.

Knight, P.G., *Glaciers* Stanley Thornes Ltd., Cheltenham,, pp. 143-145, 1999.

McCreery, C.S., F. K. Duennebier, and G. H. Sutton, Correlation of deep ocean noise (0.4–30 Hz) with wind, and the Holu Spectrum—A worldwide constant, *J. Acoust. Soc. Am.,* **93**, 2639–2648, 1993.

McDonald, B.E., Michael D. Collins, W. A. Kuperman, and Kevin D. Heaney, Comparison of data and model predictions for Heard Island acoustic transmissions, *J. Acoust. Soc. Am.* **96**, 2357-2370,1994.

Menzies, J. ,The dynamics of ice flow, in: J. Menzies (Ed.), Modern Glacial Environments: Processes, Dynamics and Sediments, Buterworth Heinemann Ltd., Oxford, pp. 139-196, 1995.

Mori, J., H. Patia, C. McFee, I. Itikarai, P. Lowenstein, P. De Saint Ours, and B. Talai, Seismicity associated with eruptive activity at Langila volcanoe, Papua New Guinea, *Jo. Vol. and Geoth. Res.,* **38**, 243, 1989.

National Ice Center, Antarctic Icebergs, http://www.natice.noaa.gov/products/ iceberg/index.htm, 2003.

National Research Council of the National Academies,, Ocean Noise and Marine Mammals, National Academies Press, Washington D.C., March 2003.

Okal, E.A., J. Talandier, O. Hyvernaud, Hydroacoustic T phases from large icebergs drifting in the Ross Sea, in: 24th Seismic Research Review-Nuclear Explosion Monitoring: Innovation and Integration, (2002) 652-665.

Polyak, L., M.H. Edwards, B.J. Coakley and M. Jakobsson, Existence of Arctic ice shelves during the Pleistocene inferred from deep-sea glaciogenic bedforms, *Nature,* **410**, 453-457, 2001.

Richardson, W.J., Greene, C.R. Jr., Malme, C.I., Thomson, D.H. (1995). Marine Mammals and Noise. Academic Press. San Diego. pp. 576.

Scambos, T., B. Raup, J. Bohlander, compilers. Antarctic ice velocity data archive, Boulder, CO: National Snow and Ice Data Center. Digital media, 2000a.

Scambos, T., C. Hulbe, M. Fahnestock, and J. Bohlander, The link between climate warming and break-up of ice shelves in the Antarctic Peninsula, J. Glaciol., 46, 516-530, 2000b.

Schlindwein, V., J. Wassermann, F. Scherbaum, Spectral analysis of harmonic tremor signals, *Geoph. Res, Let.*, **22**, 1685, 1995.

Shang, E.C., Y.Y. Wang, and T.M. Georges, Dispersion and repopulation of the Heard-Ascension modes, *J. Acoust. Soc. Am.* **96**:2371-2379, 1994.

Talandier, J., O. Hyvernaud, E. A. Okal, and P-F Piserchia, Long range detection of hydroacoustic signals from large Icebergs in the Ross Sea, Antarctica, *Ear. and Plan. Sci. Let.*, **203**:519, 2002.

Talandier, J., E.A. Okal, On the mechanism of conversion of seismic waves to and from T waves in the vicinity of island shores, *Bull. Seis. Soc. Am.*, **88**, 621-632, 1998.

Talandier, J., and E.A. Okal, Seismic detection of underwater volcanism: the example of French Polynesia, Pure Appl. Geophys., 125, 919-950, 1987.

Tolstoy, M., and D.R. Bohnenstiehl, Analysis of Hydroacoustic Signals in the Indian Ocean, *24th Seismic Research Review, Nuclear Explosion Monitoring: Innovation and Integration,* Sept. 2002.

Tolstoy, M., D.R. Bohnenstiehl, and E. Chapp, Indian Ocean Annual Catalog and Noise Report for 2002, Report for *Defense Threat Reduction Agency*, 1-59, August 2003.

Tolstoy, M., and D.R. Bohnenstiehl, Location, Characterization and Quantification of Hydroacoustic Signals in the Indian Ocean, Annual Report for *Defense Threat Reduction Agency*, 1-10, November 2003.

Tolstoy, M., D.R. Bohnenstiehl, and E. Chapp, Long Range Acoustic Propagation of High Frequency Energy in the Indian Ocean from Icebergs and Earthquakes, *26th Seismic Research Review, Trends in Nuclear Explosion Monitoring,* Sept. 2004.

Symbols, Abbrevations and Acronyms

ACZ – Antarctic Convergence Zone

CL – Cape Leeuwin

CPT – Cusped Pulsed Tremor

DGN – Diego Garcia North

DGS – Diego Garcia South

EAIC – Eastern Antarctic Ice Shelf

H01W – Cape Leeuwin

H08N – Diego Garcia North

H08S – Diego Garcia South

IMS – International Monitoring System

PSD – Power Spectral Density

SEIR – South East Indian Ridge

VHT – Variable Harmonic Tremor